

# Hair is complicated: Gravitational waves from stable and unstable boson-star mergers

Bo-Xuan Ge , <sup>\*</sup> Eugene A. Lim , <sup>†</sup> Ulrich Sperhake , <sup>2,3,4</sup> Tamara Evstafyeva , <sup>2,5,‡</sup> Daniela Corsi , <sup>2,§</sup> Eloy de Jong , <sup>¶</sup> Robin Croft , <sup>6,\*\*</sup> and Thomas Helfer , <sup>7,††</sup>

<sup>1</sup> *Theoretical Particle Physics and Cosmology Group, Physics Department, Kings College London, Strand, London WC2R 2LS, United Kingdom*

<sup>2</sup> *Centre for Theoretical Cosmology, Department of Applied Mathematics and Theoretical Physics, University of Cambridge, Wilberforce Road, Cambridge CB3 0WA, United Kingdom*

<sup>3</sup> *Department of Physics and Astronomy, Johns Hopkins University, 3400 North Charles Street, Baltimore, Maryland 21218, USA*

<sup>4</sup> *TAPIR 350-17, Caltech, 1200 E. California Boulevard, Pasadena, California 91125, USA*

<sup>5</sup> *Perimeter Institute for Theoretical Physics, Waterloo, Ontario N2L 2Y5, Canada*

<sup>6</sup> *Dipartimento di Fisica, Sapienza Università di Roma, Piazzale Aldo Moro 5, 00185, Roma, Italia*

<sup>7</sup> *Institute for Advanced Computational Science, Stony Brook University, Stony Brook, NY 11794 USA*

We explore the gravitational-wave emission from head-on collisions of equal-mass solitonic boson-star binaries from simulations spanning a two-dimensional parameter space, consisting of the central scalar-field amplitude of the stars and the solitonic potential parameter. We report the gravitational-wave energies emitted by boson-star binaries which, due to their combination of moderately high compactness with significant deformability, we often find to be louder by up to an order of magnitude than analogous black-hole collisions. The dependence of the radiated energy on the boson-star parameters exhibits striking needle-sharp features and discontinuous jumps to the value emitted by black-hole binaries. We explain these features in terms of the solitonic potential and the stability properties of the respective individual stars.

## I. INTRODUCTION

Over the past 50 years, compact objects have acquired a center-stage role in many areas of astrophysics and fundamental physics. Neutron stars (NSs) [1, 2] form the end product of the evolution of moderately massive stars and, through binary coalescence, give rise to short gamma-ray bursts [3, 4]. Supermassive BHs residing at the center of most (if not all) galaxies are intricately related to their host dynamics and evolution [5] and can drive some of the most luminous objects in the universe [6]. NSs and stellar-mass BHs, when accreting matter from a binary companion, manifest themselves as bright X-ray sources [7] and so-called *primordial* BHs are hypothesized as possible remnants of the early stages of cosmological evolution [8]. At a fundamental level, NSs represent unique laboratories to study the equation of state of matter at super-nuclear densities [9–11] while BHs, through their rotation rates, may provide us with information about matter fields beyond the standard model of particle physics [12–14]. Both, NSs and BHs enable us to test general relativity in the strong-field regime [15, 16] and, as mathematical solutions, have been essential in deepening our understanding of Einstein’s theory of general

relativity; the Schwarzschild solution in Kruskal-Szekeres coordinates or the Buchdahl limit are prominent points in case. On the observational side, the exploration of compact objects has received a tremendous boost from the direct detection of gravitational waves (GWs) by the Laser Interferometer Gravitational-Wave Observatory (LIGO) and Virgo [17, 18].

One of the most exciting questions in this context is the very nature of compact objects and whether these encompass *exotic* members composed of matter beyond the standard model of particle physics. Exotic compact objects may furthermore constitute a significant fraction of the enigmatic *dark matter* content of the universe, either themselves or as localized concentrations indicative of fundamental fields permeating spacetime on grander scales. While a plethora of experiments has been searching for dark-matter candidate fields [19–21], their capacity to form gravitationally bound macroscopic concentrations or “stars” offers the unique opportunity to study them as compact-binary sources of GWs. Such an observational effort, however, requires a detailed theoretical understanding and precision modeling of exotic compact binaries for two main reasons. First, the canonical approach to analyze observational data from GW detectors is based on Bayesian statistics and matched filtering techniques employing extensive theoretical GW template banks [22, 23]. Second, as evidenced in Ref. [24] for the case of boson stars and the sensitivity of present GW detectors, the GW signals generated by the inspiral and coalescence of exotic compact binaries can exhibit significant degeneracy with those from black-hole (BH) binaries. Breaking this degeneracy through the identification

<sup>\*</sup> bo-xuan.ge@kcl.ac.uk

<sup>†</sup> eugene.a.lim@gmail.com

<sup>‡</sup> te307@cam.ac.uk

<sup>§</sup> dc889@cam.ac.uk

<sup>¶</sup> eloydejong93@gmail.com

<sup>\*\*</sup> robin.croft@uniroma1.it

<sup>††</sup> thomashelfer@live.de

of characteristic signatures from exotic compact objects will be of great benefit in our GW guided quest for new physics.

The main goal of this paper is to explore in depth specific characteristics of the GW emission from stars composed of a complex scalar field. This class of compact objects, henceforth referred to simply as *boson stars* (BSs) (see e.g. Refs. [25–27] for reviews), combines a deceptive simplicity regarding their mathematical foundation with a remarkably rich phenomenology of their dynamics and radiative properties. As such, BSs are not only interesting in their own right, but also provide an excellent proxy to capture main effects for a wider range of compact objects. Put another way, should the analysis of a future GW event exhibit statistically significant preference for BS templates relative to BH ones, the impact would be substantial whether or not the source eventually turns out to be a BS or another exotic source as for example cosmic strings [28] or compact stars composed of higher-spin fields [29].

The concept of BSs first appeared almost 60 years ago thanks to the pioneering work by Kaup [30], whilst their dynamics in binary systems have been studied numerically with increasing intensity only for about 20 years. These studies have already uncovered a considerable amount of valuable insight on the properties of these exotic objects by focusing on binaries consisting of rotating stars [31–39], BSs with light rings [40–43], equal- [44–51] and unequal-mass binaries [52–54], hybrid BS-NS [55] and BS-BH [56, 57] binaries, multiple scalar fields [58–64], real scalar fields (aka *oscillatons*) [65–68] and vector fields (aka *Proca stars*) [29, 69–71]. The BS parameter space offers ample avenues for further exploration. For example, the impact of dephasing and the vortex structure on the dynamics of inspiralling BS binaries has only recently been studied in Ref. [72]. Their results demonstrate for the first time that a rotating BS can form from the coalescence of two non-spinning BSs. Formation of these objects are less well studied, but in [73], it was shown that real-scalar stars can generically form from the collapse of overdense regions. Similarly, thanks to increased efforts to model exotic compact objects more extensively, a surrogate model for equal-mass head-on collisions of Proca stars has been constructed in Ref. [74].

The merger dynamics of BS binaries have been found to exhibit a (perhaps surprisingly) rich phenomenology driven by the specific properties of the individual BSs. For instance, Ref. [75] observes that the GW emission of the simulated head-on collisions of equal-mass mini BSs is quadrupole dominated but with varying characteristics. On the one hand, in-phase BSs merge into a single more massive star whereas, on the other hand, binaries with maximally dephased scalar fields come close to each other but remain separate, almost like two touching snooker balls. For large initial momenta, the two mini BSs can even pass through each other [67, 76], exhibiting a true solitonic nature. An even more exotic fate of an

inspiralling BS binary has been found in Ref. [53], where an aligned-spin binary, instead of merging, forms a binary of nonspinning BSs flung out away from the center of mass. Ultrarelativistic BS collisions were modeled in Ref. [77] and found to result in BH formation, consistent with predictions by Thorne’s hoop conjecture [78].

Numerical explorations of BSs have thus demonstrated many interesting features of their mergers and dynamics; however, our insight is largely limited to isolated points or patches in the BS parameter space leaving systematic explorations of the complete parameters as a key challenge for complementary work. The most comprehensive study in this direction has, to our awareness, been performed for Proca stars in Ref. [79], covering a range of frequency (i.e. mass) ratios and phase offsets. The central goal of our work is to extend the parameter coverage to the potential function for head-on collisions of equal-mass non-spinning scalar BSs. For this purpose we simulate  $\sim 10^4$  BS merger systems composed of a scalar field of mass  $m$  self-interacting through a solitonic potential

$$V(\phi) = m^2 |\phi|^2 \left(1 - 2 \frac{|\phi|^2}{\sigma^2}\right)^2, \quad (1)$$

where  $\sigma$  is the self-interaction parameter. Specifically, we consider a two-dimensional hypersurface of the parameter space spanned by  $\sigma$  and the BS compactness controlled through the central scalar-field amplitude  $|\phi_c|$ . Across this parameter range, we monitor the BS dynamics through infall and merger, the nature of the remnant and, most importantly, the resulting GW emission.

Throughout this work, we employ natural units where  $\hbar = 1 = c$  but keep the gravitational constant  $G$  related to the Planck mass by  $M_{\text{Pl}} = \sqrt{G}^{-1}$ .

## II. EXECUTIVE SUMMARY

The précis of our findings is presented in Fig. 1 where we plot for  $\sigma = 0.28725 M_{\text{Pl}}$  the GW energy, normalized by the total BS mass  $M_{\text{tot}} = M_1 + M_2 =: 2M$ , generated in the head-on collision of two BSs with central scalar-field amplitude  $|\phi_c|$ , initial separation  $80 m^{-1}$  and initial velocity  $v = 0.1$  towards each other. This figure demonstrates several remarkable features which we will discuss and explain in physical terms in this paper.

- (1) *BS collisions can be radiatively way more efficient than those of BHs.* The GW energy released in the BS collisions reaches values up to  $E_{\text{GW}}/M_{\text{tot}} = 0.0035$ , about six times larger than the corresponding number  $6 \times 10^{-4}$  observed in head-on collisions of non-spinning equal-mass BHs; see e.g. Fig. 4 in Ref. [80] and also compare with the red dots in our Fig. 1 where the BSs have collapsed to BHs prior to merger. We will encounter yet larger energies when we discuss other  $\sigma$  values later on. This effect was first noted in Ref. [65] in the context of

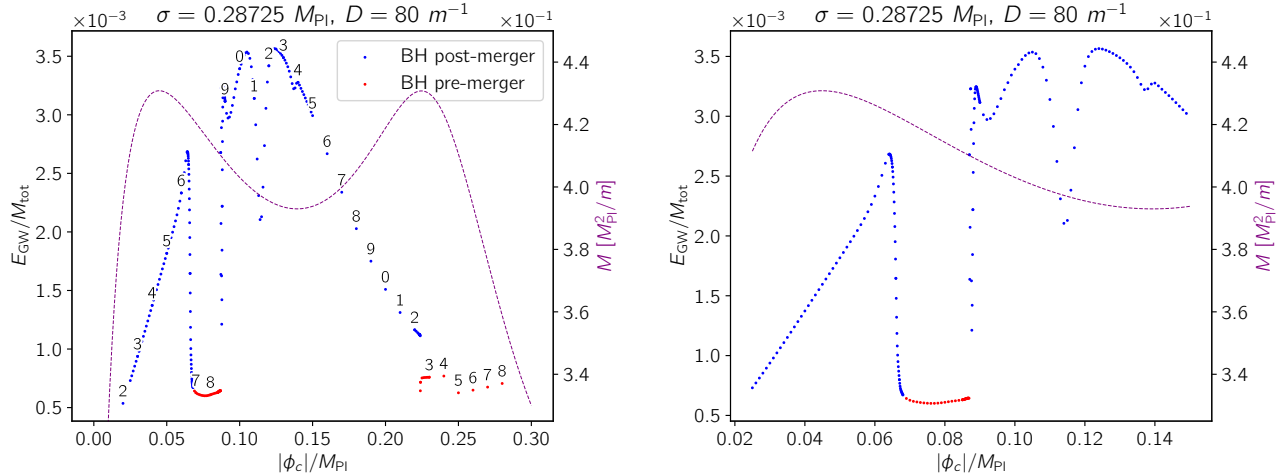


FIG. 1. *Left:* The GW energy of the head-on collision of two BSs with a solitonic potential (1) for  $\sigma = 0.27825 M_{\text{Pl}}$  is shown as a function of the BSs' central scalar-field amplitude  $|\phi_c|$ . Blue dots represent binaries completing their infall as BSs and forming a BH or BS at merger whereas red symbols denote systems where each BS collapses to a BH prior to merger. The numbers adjacent to the dots give the final digit of their  $|\phi_c|$  value. The purple line represents the mass curve  $M(|\phi_c|)$  for single spherical BSs with central scalar-field amplitude  $|\phi_c|$ . *Right:* Zoom into the region around the sharp variations of  $E_{\text{GW}}(|\phi_c|)$ .

self-gravitating real-scalar-field oscillatons, suggesting that this is a generic effect for mergers of compact objects composed of fundamental fields.

- (2) *There are discontinuities in the GW energy viewed as a function of  $|\phi_c|$ , i.e. the BS compactness.* At  $|\phi_c|/M_{\text{Pl}} \gtrsim 0.08$ , the energy  $E_{\text{GW}}$  abruptly jumps from the BH value  $E_{\text{GW}}^{\text{BH}} \approx 6 \times 10^{-4} M_{\text{tot}}$  (red dots) to about twice this value (the next right blue dot). Between  $|\phi_c|/M_{\text{Pl}} = 0.22$  and  $0.23$ , the function  $E_{\text{GW}}(|\phi_c|)$  exhibits a further discontinuity; even though this jump is relatively small, it is well resolved by our numerics.
- (3) *Even away from these discontinuities, small differences in the initial configuration lead to large, albeit continuous,  $\mathcal{O}(1)$  differences in the GW emission.* The functional dependence of the GW energy on  $|\phi_c|$  exhibits sharp local extrema, most notably the local minimum at  $|\phi_c|/M_{\text{Pl}} \approx 0.115$ ; we will find these sharp extrema – maxima or minima – to be even more prominent for other  $\sigma$  values and, henceforth, refer to them as *needles*. This observation suggests that it can be misleading to assume similar BS collisions produce approximately equal output in GWs.
- (4) *We discern significant correlation – overall positive for small and negative for large  $|\phi_c|$  – of the radiated energy  $E_{\text{GW}}(|\phi_c|)$  when compared to the mass function  $M(|\phi_c|)$ .* We will show how this correlation can be explained in terms of the shape of the potential  $V(|\phi_c|)$  and that  $E_{\text{GW}}(|\phi_c|)$  must be extremal near the minimum of the mass function  $M(|\phi_c|)$  provided there exist stable BSs in a neighbourhood to the right of this  $|\phi_c|$  value.

Our discussion of these effects is organized as follows. In Sec. III we summarize our computational setup and

calibrate the numerical uncertainty. The structure and stability of single BSs and their solution branches is analyzed in Sec. IV and in Sec. V, we present the key findings of our investigation of BS collisions and their GW emission. We discuss our findings in Sec. VI and present some details of the GW extraction in the appendix.

### III. THEORY AND COMPUTATIONAL FRAMEWORK

BSs composed of a single complex scalar field  $\phi$  minimally coupled to the spacetime metric  $g_{\alpha\beta}$  of general relativity are described by the Lagrangian

$$\mathcal{L} = \frac{1}{16\pi G} R - \frac{1}{2} g^{\mu\nu} \nabla_\mu \bar{\phi} \nabla_\nu \phi - \frac{1}{2} V(\phi), \quad (2)$$

where an overbar denotes the complex conjugate and  $V$  is the potential function given in our case by Eq. (1). Variation of the action  $S = \int \sqrt{-g} \mathcal{L} d^4x$  with respect to the metric and scalar field results in the covariant equations

$$\begin{aligned} G_{\alpha\beta} &= 8\pi G \left\{ \nabla_{(\alpha} \bar{\phi} \nabla_{\beta)} \phi - \frac{1}{2} [\nabla^\mu \bar{\phi} \nabla_\mu \phi + V(\phi)] \right\}, \\ \nabla^\mu \nabla_\mu \phi &= \frac{dV}{d|\phi|^2} \phi. \end{aligned} \quad (3)$$

The calculation of spherically symmetric single-BS spacetimes is most conveniently performed by decomposing the scalar field into amplitude and phase according to

$$\phi(t, r) = |\phi(r)| e^{i\omega t}, \quad (4)$$

where  $|\phi(r)|$  is the scalar-field amplitude and  $\omega$  the (constant positive) frequency. This ansatz can be generalized

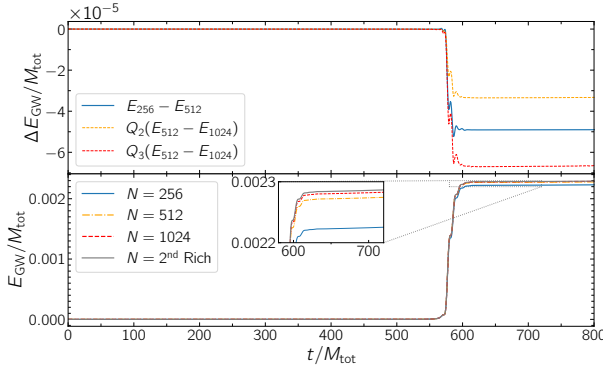


FIG. 2. Convergence analysis of the GW energy for the binary BS configuration  $\sigma = 0.25 M_{\text{Pl}}$ ,  $|\phi_c| = 0.18 M_{\text{Pl}}$ . The top panel displays the differences in the energy as a function of time for resolutions  $N = 256$ ,  $N = 512$  and  $N = 1024$  points with the higher-resolution differences magnified by factors  $Q_2 = 4$  and  $Q_3 = 8$  expected for second and third-order convergence. The bottom panel shows the radiated energy as a function of time for all resolutions together with the result for second-order Richardson extrapolation.

by writing the phase factor as  $e^{i(\epsilon\omega t + \delta\vartheta)}$ , where  $\epsilon = \pm 1$  distinguishes BSs and anti-BSs, and  $\delta\vartheta$  denotes a phase shift. In this work, we exclusively consider BS binaries without phase offset and, hence, set  $\epsilon = 1$ ,  $\delta\vartheta = 0$ . With the decomposition (4), the Einstein-Klein-Gordon equations for a spherically symmetric metric

$$ds^2 = -\alpha(r)^2 dt^2 + X(r)^2 dr^2 + r^2(d\theta^2 + \sin^2\theta d\varphi^2),$$

result in a coupled set of four first-order ordinary differential equations which we solve with a shooting method as detailed in Sec. 2.3 of Ref. [44]; cf. also Appendix A of Ref. [81] for an in-depth discussion of the solution's asymptotic behaviour at infinity.

For BS binary evolutions, we construct initial data by combining two such single-BS spacetimes using the *constant volume element* technique of Refs. [44, 52, 65]; cf. also Ref. [47]. This technique results in a significant improvement in the Hamiltonian constraint equation over the simple linear superposition of the two BS solutions.

The resulting binaries are characterized by the parameter  $\sigma$  in the solitonic potential (1), the stars' central scalar-field amplitudes  $|\phi_c|$ , their initial separation  $D$  and their velocities  $v$ . Our study focuses on non-spinning equal-mass BS binaries, so that both stars have equal  $|\phi_c|$  and, in the rest frame used for all our runs, their initial velocity has equal magnitude with direction pointing toward each other. Unless specified otherwise, we fix  $v = 0.1$  and  $D = 80 m^{-1}$  which leaves us with two control parameters,  $\sigma$  and  $|\phi_c|$ . In this paper, we present results for  $\sigma/M_{\text{Pl}} = \{0.25, 0.28725, 0.3, 0.5\}$  as well as the mini-BS limit  $\sigma \rightarrow \infty$ ; these cases are fully representative of the dynamics under consideration, but we note that further values of  $\sigma$  are discussed in Ref. [82].

We simulate the head-on collisions resulting from these initial data using the GRCHOMBO code [83–85] which

evolves the Einstein equations in the CCZ4 formulation [86]. Our specific version of the CCZ4 equations is given in Sec. 2 of Ref. [84] and is discretized using the *method of lines* with fourth-order finite differencing in space and a fourth-order Runge-Kutta scheme in time. GRCHOMBO implements Berger-Rigoutsos adaptive-mesh refinement provided by the CHOMBO library [87] and facilitates various tagging criteria for the grid generation as summarized in Sec. 3 of Ref. [84]. In this paper, we utilize the scalar field  $|\phi|$  and the conformal factor  $\chi$  for regridding with their respective thresholds set to 0.3. We exploit the inherent axisymmetry of our BS binary configurations by reducing our computational domain from three to two spatial dimensions using the *modified cartoon method* in the form detailed in Ref. [88]; cf. also [89, 90] as well as Appendix B for our cartoon implementation of the wave extraction. This combination of mesh refinement and dimensional reduction enables us to simulate approximately 10 000 simulations – each utilizing two nodes (56 logical cores) and lasting approximately four hours. We employ a domain of length  $512 m^{-1}$  and a grid setup consisting of a nested set of  $L = 7$  refinement levels with grid spacing  $dx = 1/(32 m)$  on the innermost level, increasing by a factor 2 consecutively on each level further out.

For the calibration of our numerical uncertainty, we have simulated a representative BS binary configuration with  $\sigma = 0.25 M_{\text{Pl}}$  and  $|\phi_c| = 0.18 M_{\text{Pl}}$  using three resolutions, our default  $N = 256$  as well as two higher resolutions  $N = 512$  and  $N = 1024$ . The result, displayed in Fig. 2, demonstrates convergence between second and third order. We conservatively estimate the discretization error by assuming second-order convergence for the Richardson extrapolation and obtain a relative error of about 2.5% for  $N = 256$ . By fitting the energy values obtained at different extraction radii with a polynomial in  $1/R_{\text{ex}}$  truncated at second order, we find an additional uncertainty of  $\sim 2\%$  at our fiducial  $R_{\text{ex}} = 140 m^{-1}$  resulting in a total error budget of  $\sim 4.5\%$ . We have also monitored the constraint violations of our simulations as described in Appendix A.

As a final test, we compare in Fig. 3 the GW signal for a BS head-on collision for  $\sigma = 0.35 M_{\text{Pl}}$  and  $|\phi_c| = 0.086 M_{\text{Pl}}$  calculated with our modified Cartoon approach with the result from a fully three-dimensional computation. The results agree within about a percent, commensurate with the uncertainty of the three-dimensional simulation [44].

## IV. SINGLE BOSON STARS

### A. Stationary boson stars

Many of the prominent features we observe in the dynamics and GW emission of BS head-on collisions find their origin in the properties of single BS spacetimes. We therefore start the discussion of our results by recalling the essential characteristics of spherically symmet-

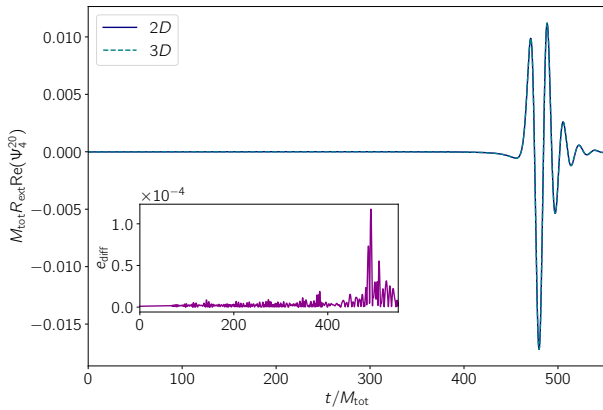


FIG. 3. Comparison of the (2,0) GW mode generated by the head-on collision of equal-mass BSs with  $|\phi_c| = 0.086 M_{\text{Pl}}$ ,  $\sigma = 0.35 M_{\text{Pl}}$  using the 2D and 3D versions of the GRCHOMBO code. The inset shows the absolute difference  $e_{\text{diff}}$  between the two signals and demonstrates relative agreement  $\lesssim 1\%$ , well within the uncertainty of the simulations.

ric, stationary BS models. For a fixed scalar potential, Eq. (1) in our case, the space of spherically symmetric solutions is controlled by the central scalar-field amplitude  $|\phi_c|$ . More specifically, for each value  $|\phi_c|$ , there exists a countably infinite number of BS models characterized by the number  $n$  of zero crossings of the radial profile  $|\phi(r)|$ : the *ground-state* BS with  $n = 0$  and the *excited*<sup>1</sup> stars for  $n = 1, 2, \dots$ . For a broad range of scalar potentials, the latter have been found to be intrinsically unstable to generic perturbations [91], but more recent studies have found that sufficiently large self-interaction terms may cure such instabilities [92, 93]. In any case, excited BSs will play no further role in this paper.

The remaining ground-state models represent a one-parameter family of BSs with each member determined by its central scalar amplitude  $|\phi_c|$ . The solution space is conveniently displayed as a curve  $M(|\phi_c|)$  in the *mass-amplitude*<sup>2</sup> plane where, analogous to the Tolman-Oppenheimer-Volkoff [94, 95] solutions for spherically symmetric NSs, it divides into stable and unstable branches [96–99]. These branches are delineated by local extrema of the function  $M(|\phi_c|)$  where the time dependence of radial perturbations changes from oscillatory to exponential [91, 100–107]. For so-called *mini BSs*, where  $\sigma \rightarrow \infty$ , composed of a non-interacting scalar field, for example, the  $M(|\phi_c|)$  curve consists of one stable ( $|\phi| < |\phi|_{\text{Kp}}$ ) and one unstable branch ( $|\phi| > |\phi|_{\text{Kp}}$ ) separated by the maximum-mass or *Kaup limit* [30] model with

$M = M_{\text{Kp}} \approx 0.633 M_{\text{Pl}}^2/m$  for  $|\phi_c| = |\phi|_{\text{Kp}} \approx 0.0765 M_{\text{Pl}}$ . For the solitonic potential (1), however, the branch structure becomes more complicated; more precisely, it mirrors the more complicated structure of the potential function  $V(|\phi|)$  itself.

We can qualitatively understand this by considering the simplified scenario of an approximately stationary and spatially uniform scalar field. The energy of such a field is dominated by the potential term  $V(|\phi|)$  and we expect it to roll towards the stable equilibrium at a local minimum of this function. Considering now the solitonic potential (1), we find three extrema, a local maximum at  $|\phi| = \sigma/\sqrt{6}$  and the two minima  $|\phi| = 0$  and  $|\phi| = \sigma/\sqrt{2}$ . The latter two correspond to stable configurations while  $|\phi| = \sigma/\sqrt{6}$  is unstable. BSs are, of course, *not* spatially uniform; instead their scalar amplitude spans the entire range from  $|\phi| = 0$  at infinite radius to  $|\phi_c|$  at the origin. And yet, let us take the analogy as qualitative guidance for the moment, making sure to have a pinch of salt at the ready.

Recalling from the above discussion of NSs and mini BSs that local extrema in the  $M(|\phi_c|)$  curve typically<sup>3</sup> mark the transition between stable and unstable models, stable BS models will be located on rising slopes of  $M(|\phi_c|)$ , i.e. have  $dM/d|\phi_c| > 0$  while unstable models mainly coincide with  $dM/d|\phi_c| < 0$ . Our crude analogy to homogeneous scalar fields would then suggest that minima (maxima) in  $V(|\phi_c|)$  coincide with rising (descending) slopes of  $M(|\phi_c|)$ .

We illustrate this behaviour in Fig. 4 for five values  $0.2 \leq \sigma/M_{\text{Pl}} \leq 0.5$  and the mini-BS limit  $\sigma \rightarrow \infty$ . There we distinguish between unstable BSs, perturbatively stable stars and globally stable BS models, the latter defined by minimizing the binding energy  $M - \mathcal{N}$  over all BS models of equal Noether charge  $\mathcal{N}$ . We see in this figure that our association of maxima in  $V(|\phi_c|)$  with unstable stars is borne out for all potentials. Our expectation that minima in  $V(|\phi_c|)$  correspond to stable stars, on the other hand, is true for  $\sigma \lesssim 0.4 M_{\text{Pl}}$  but only holds for the true vacuum  $|\phi_c| = 0$  when  $\sigma \gtrsim 0.4 M_{\text{Pl}}$ . In this latter regime, the false vacuum state  $|\phi| = \sigma/\sqrt{2}$  has shifted to rather large values corresponding to very compact stars where gravitational effects dominate over scalar self interaction and our simplified model evidently starts showing cracks.

We summarize our observations by displaying schematically in Fig. 5 the first three (in the sense of  $|\phi_c|$  increasing from 0 towards positive values) extrema of the  $M(|\phi_c|)$  curves computed in Fig. 4. These extrema naturally divide the  $|\phi_c|$  parameter range into four regions, labeled I to IV, where, alternatingly,  $dM/d|\phi_c| > 0$  for odd

<sup>1</sup> Not to be confused with “perturbed” or “dynamic” BSs which are stars evolving in time. Excited BSs, in contrast, are equilibrium solutions merely having one or more zero crossings in their radial scalar-field profile.

<sup>2</sup> Alternatively, the solutions can be represented in a mass-radius or  $M(R)$  diagram.

<sup>3</sup> The rule is not rigorous; for example increasing  $|\phi_c|$  well beyond the Kaup limit for mini BSs ultimately leads to further extrema in  $M(|\phi_c|)$  for ultra-compact BSs, none of them marking a return to stable BSs. The presence or absence of a change in stability depends on whether the static perturbation belongs to the fundamental radial oscillation mode or an overtone [102].

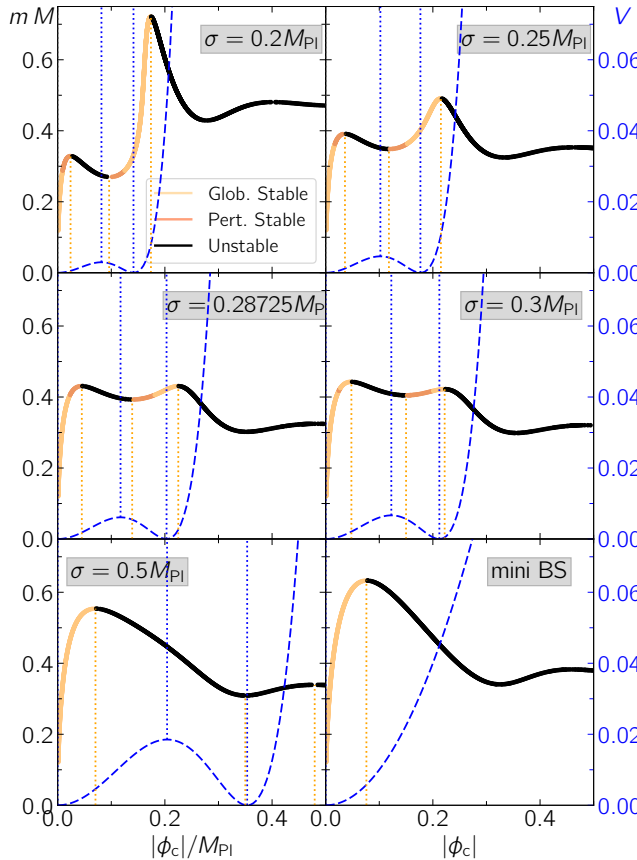


FIG. 4.  $M(|\phi_c|)$  diagrams for the one-parameter families of BSs obtained for  $\sigma/M_{\text{Pl}} = 0.2, 0.25, 0.28725, 0.3, 0.5$  as well as the mini-BS limit  $\sigma \rightarrow \infty$ . For each one-parameter family of BS models, globally (perturbatively) stable models are displayed in light (dark) copper color while unstable stars are marked in black. The blue dashed curves, quantified in units of  $m^2 M_{\text{Pl}}^2$  on the right vertical axis, represent the respective potential functions (1). The vertical dotted lines mark the extrema of the potential (blue) and the mass-amplitude curves (orange).

and  $dM/d|\phi_c| < 0$  for even region number. BS models in region I are always stable whereas BS models in regions II and IV are always unstable. Models in region III are stable *provided* they are not too compact; otherwise they are unstable. The structure of the branches and their relative height furthermore suggest the following possible fates for unstable stars perturbed out of equilibrium.

- (i) The BS evaporates with the entire scalar-field matter dispersing to future timelike infinity  $i^+$ .
- (ii) The BS sheds part of its matter and migrates to a stable model with lower mass.
- (iii) The BS migrates to a more compact stable configuration with equal Noether charge.
- (iv) The BS collapses to a BH.

Roughly speaking we may consider this sequence of scenarios as pointing in the direction from the scalar-

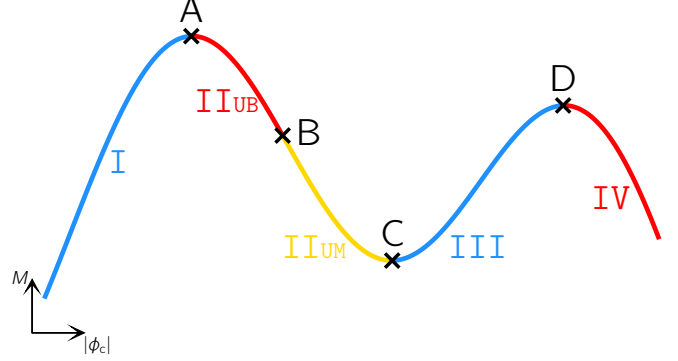


FIG. 5. Schematic illustration of the  $M(|\phi_c|)$  curve and the resulting branches for stationary BSs. The local extrema naturally divide the  $|\phi_c|$  range into regions I and III with  $dM/d|\phi_c| > 0$  and regions II and IV with  $dM/d|\phi_c| < 0$ . BSs of the former regions – provided they are not extremely compact – are stable (marked in blue) while the latter regions are exclusively comprised of unstable stars which, when perturbed, either collapse to BHs (red) or migrate to more compact stable BS configurations (yellow). We correspondingly call these branches **S** (stable), **UB** (unstable BH) and **UM** (unstable migrating).

dominated to the gravity-dominated regime. Empirically, as discussed in detail in the next subsection, we exclusively observe cases (iii) and (iv); we suspect that the shedding of matter or evaporation, while theoretically possible, requires delicately fine tuned initial perturbations corresponding to a bulk outward motion of the matter. The possibility of migration to a more compact stable BS naturally depends on the existence of such models and, therefore, on the relative height of the two bumps in the  $M(|\phi_c|)$  curve. In the following, we label the three relevant branch types of Fig. 5 as **S** (stable), **UM** [unstable migrating, corresponding to the above scenario (iii)] and **UB** [unstable BH, corresponding to scenario (iv)].

## B. Time evolutions of single boson stars

We investigate the dynamical behaviour of BSs from the three branch types by evolving them in time with the numerical methods detailed in Sec. III. Here the instability is triggered by imperfections in the initial data and/or discretization of the evolution equations, but their particular nature is of significance only in so far as they are of the same kind for all configurations. In our analysis of these numerical simulations, we use the following diagnostics.

1. We monitor the maximum scalar-field amplitude  $|\phi|_{\text{max}}$  on the spatial domain as a function of time; we always find this maximum to be realized at the BS center.
2. We define the moment when  $|\phi|_{\text{max}}$  deviates from its

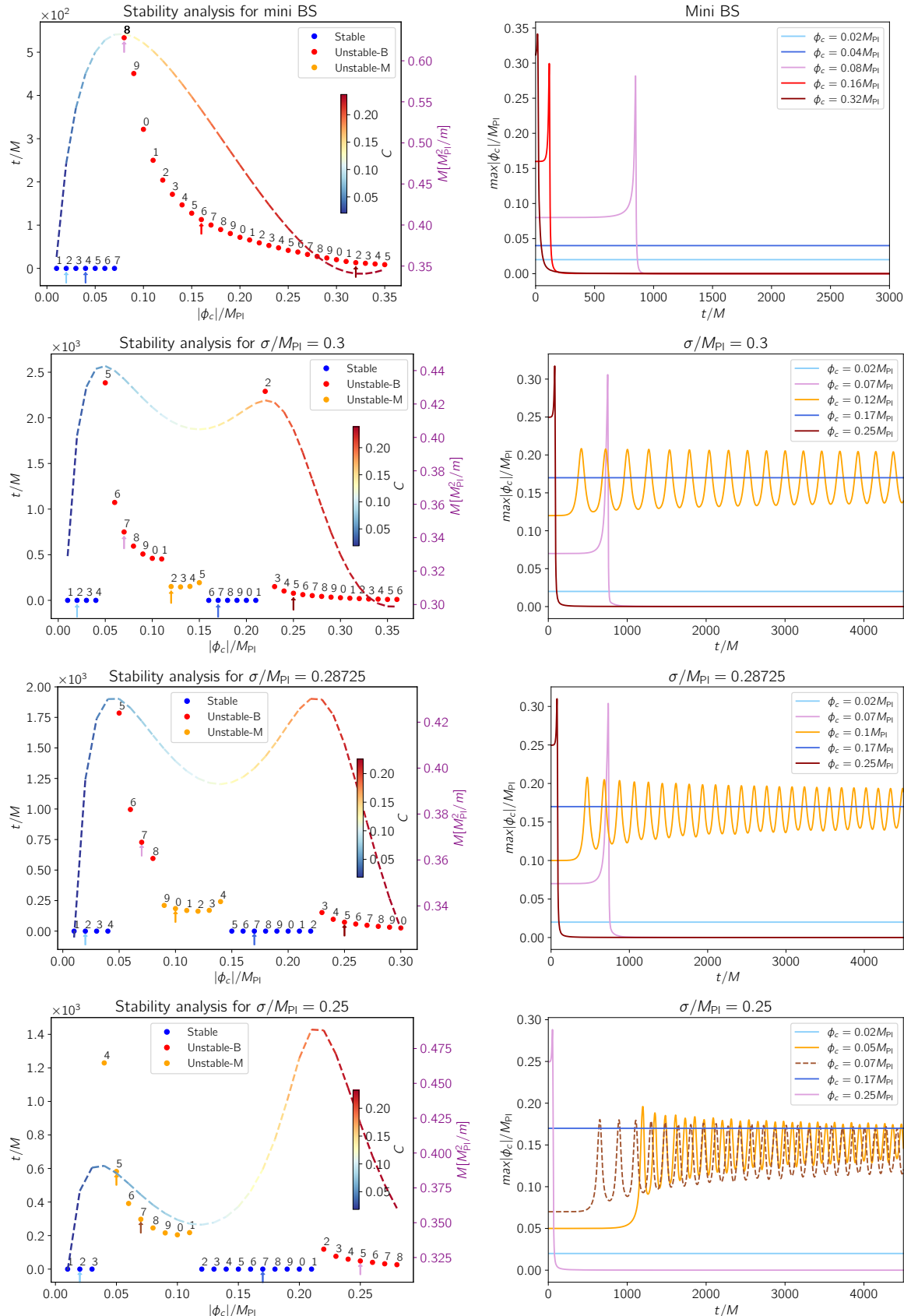


FIG. 6. *Left panels:* The  $M(|\phi_c|)$  curve, plotted for  $\sigma/M_{\text{Pl}} = \infty$ , 0.3, 0.28725, 0.25, encodes in color the BS compactness  $C$ . The vertical axis on the left (right) marks the migration time (mass of the BS). The stability properties for selected stars are marked by colored symbols: blue for stable **S** branch stars, red for **UB** stars collapsing to a BH, orange for **UM** stars migrating to a more compact BS and their vertical position represents the migration time. The numbers adjacent to the symbols give the final digit of their  $|\phi_c|$  value, whilst the arrows underneath highlight the models illustrated in the corresponding right panels. *Right:* The time evolution of the scalar amplitude maximum,  $|\phi|_{\max}(t)$ .

initial value by 0.1 % as the *migration time*.

3. We monitor the minimum value of the CCZ4 conformal factor function  $\chi$  on the spatial domain as a function of time. If  $\chi_{\min}$  drops below 0.1, we conclude formation of a BH. We independently verify this by checking that the scalar amplitude  $|\phi|_{\max}$  exhibits a rapid drop to zero as the scalar field collapses into a singular point that is not resolved numerically. We always find both BH indicators in agreement.
4. We quantify the compactness of equilibrium BSs as the maximal ratio of the mass aspect to areal radius,  $C := \max_{r \geq 0} \frac{M(r)}{r}$ .

The results of this analysis are summarized in Fig. 6, which displays the evolution of BSs across a wide range of compactness for the mini BS potential  $\sigma \rightarrow \infty$  and the solitonic cases  $\sigma/M_{\text{Pl}} = 0.3, 0.28725$  and  $0.25$ .

Let us first consider the case of mini BSs shown in the top row of the figure. In complete agreement with Fig. 4, the global maximum, i.e. Kaup limit, at  $|\phi_c| \approx 0.0765 M_{\text{Pl}}$  separates the stable and unstable branches: all models to the left of this point stay in their initial configuration (the blue symbols placed at migration time  $t = 0$ ) whereas all models to the right collapse to BHs (red symbols, marking **UB** instability). As expected, the migration time away from their initial state exhibits a pole at the Kaup limit, commensurate with the vanishing of the fundamental radial eigenmode's frequency<sup>4</sup> [102], and rapidly drops with increasing compactness. In our simulations, models beyond the mass minimum at  $|\phi_c| \approx 0.33$ , despite being on the potentially stable branch III of Fig. 5, ubiquitously collapse to BHs as shown by the time evolutions  $|\phi|_{\max}(t)$  for selected BSs in the top right panel.

As we decrease  $\sigma$  in the following rows of Fig. 6, we see the second bump in the  $M(|\phi_c|)$  curve moving towards smaller  $|\phi_c|$  and substantially increasing in magnitude. For all cases  $\sigma \leq 0.3$ , this second bump results in two sets of stable BSs – cf. the blue dots in the left panels of Fig. 6 – corresponding to branches I and III of Fig. 5. All models beyond the second bump, i.e. all models belonging to branch IV, are unstable and ubiquitously collapse to BHs (red dots); for the cases  $\sigma \leq 0.3$  in Fig. 6, this transition to branch IV occurs at  $|\phi_c| \approx 0.22$ .

The most complex behavior arises for the moderately compact stars on branch II where  $dM/d|\phi_c| < 0$ . For  $\sigma = 0.3$  and  $\sigma = 0.28725$ , this branch II hosts **UB** models collapsing to a BH on its left end and **UM** models on its right end which migrate to a more compact stable BS. Evidently, this behavior depends on the height of the second bump in the  $M(|\phi_c|)$  curve relative to the first: initial configurations on branch IIUM, i.e. deep down in

the trough, have relatively low mass and can migrate horizontally<sup>5</sup> at approximately fixed  $M$  to the right where they find a stable configuration to settle down to. In the right panels of the figure, these stars exhibit a sudden increase in the scalar  $|\phi|_{\max}(t)$  followed by a slowly damped oscillation around the target configuration's equilibrium value. BSs starting on branch IIUB (further left), in contrast, have too large a mass to find their collapse halted by a stable BS configuration on the second bump and thus are doomed to form a BH. In practice, we generically find this **UB** segment of branch II to extend a bit further to the right than would be expected from the height of the second bump; we believe this to result from an overshooting of the dynamical compression of the star beyond the compactness of its stable equilibrium cousin with equal Noether charge. Finally, for the case  $\sigma = 0.25$ , the second bump has become so much larger relative to the first one that the **UB** part of branch II has disappeared; every branch II star now migrates to a stable BS configuration on branch III.

## V. BS COLLISIONS

### A. General behaviour

The first and perhaps most elementary of our observations in Fig. 1 is *the enhanced radiative efficiency of BS collisions as compared to their BH counterparts*. This has already been noticed for oscillations in Ref. [65] (see their Fig. 1) and in Ref. [52] for unequal-mass BS collisions (see their Fig. 9). We interpret this feature in terms of two competing effects: the GW emission is expected to increase with (i) the binary constituents' compactness and (ii) a higher degree of asymmetry around merger. BSs, being less compact but more vulnerable to deformation at merger than BHs, are thus expected to have their radiative efficiency reduced by the first effect but enhanced by the second. Empirically, our results confirm the observations of the above literature, namely that the net effect is optimized for moderate compactness considerably below that of BHs. In this section, we will for now assert this empirical result which we colloquially phrase as “mergers of deformable BSs are louder<sup>6</sup>” in order to capture the fact that GW efficiency depends on both, compactness and the tendency of BSs to deform into highly asymmetrical configurations during merger. We will then return to conjecture on its origin in section V B.

Guided by the stability properties and corresponding migration or collapse tracks of single BSs as summarized

<sup>4</sup> We note Ref. [108] reports that extremal-mass configurations do not necessarily correspond to zero-frequency modes; our findings neither confirm nor contradict their results.

<sup>5</sup> Strictly speaking, the migration is not exactly horizontal in this diagram because the Noether charge, rather than the BS mass, is conserved; the two quantities are typically comparable in magnitude, however, so that the migration occurs horizontally to leading order.

<sup>6</sup> Obviously, when the BS are *too* squishy, they approach the weak field limit and GW production becomes less efficient.

in Fig. 6, we now aim to understand the remaining phenomenology of the GW emission in head-on collisions of BSs listed at the end of Sec. II: discontinuities in the functional relation  $E_{\text{GW}}(|\phi_c|)$ ; the “needles”, i.e. large and very sharp swings in the total GW energy as one varies  $|\phi_c|$  for a fixed potential  $V(|\phi|)$ ; the correlation between  $E_{\text{GW}}(|\phi_c|)$  and  $M(|\phi_c|)$ .

For this purpose, we first summarize in Fig. 7 the main types of mergers suggested by our stability analysis of Fig. 6; there are three such types. (1) The initial BSs are stable, remain in equilibrium until merger where they coalesce into a BS or BH remnant. (2) The initial BSs are unstable, each of them collapses to a BH, and thenceforth they complete their coalescence as a BH binary. (3) The initial BSs are unstable but migrate towards a stable BS configuration around which they oscillate in dynamic fashion; upon merging, they form a BH remnant<sup>7</sup>.

We next consider the repercussions of these three possible merger scenarios in the context of our schematic stability Figure 5. Starting from the left (small  $|\phi_c|$ ), we encounter the following qualitative screenplay.

**Branch I:** On branch I, we have stable BSs merging according to case 1 into a BS or BH remnant. In consequence of the competing effects of increasing compactness and decreasing susceptibility to deformation, we expect the GW energy  $E_{\text{GW}}$  to rise as  $|\phi_c|$  is increased from 0, possibly peaking at some optimal compactness.

**Branch II<sub>UB</sub> (red):** Beyond point A, i.e. the first maximum in the  $M(|\phi_c|)$  curve of Fig. 5, we reach the red patch of the unstable branch II; our initial BSs are unstable, collapse to individual BHs during infall and form a BH merger remnant at coalescence according to the case 2 scenario of Fig. 7. The radiated energy function  $E_{\text{GW}}(|\phi_c|)$  should consequently exhibit a discontinuous jump from a large BS value to the generic  $E_{\text{GW}}^{\text{BH}} \approx 6 \times 10^{-4} M_{\text{tot}}$ , as has already been observed for head-on collisions of oscillations [65].

Let us next connect these theoretical expectations with the results from the actual BS collisions displayed in Fig. 1. There we indeed observe the expected increase in  $E_{\text{GW}}(|\phi_c|)$  at low compactness. The curve furthermore exhibits a local maximum before rapidly dropping to  $E_{\text{GW}}^{\text{BH}} \approx 6 \times 10^{-4} M_{\text{tot}}$  marked by the red dots around  $0.068 \lesssim |\phi_c|/M_{\text{Pl}} \lesssim 0.083$ . Contrary to our expectation, however, this rapid drop occurs at  $|\phi_c|$  values *beyond* the maximum mass (cf. the dashed purple curve in the figure). As we will discuss in more detail in Sec. V D, this discrepancy between our results and theoretical expectations is a consequence of the finite infall time which, for marginally unstable BSs, is insufficient for the stars to complete their collapse to a BH; binaries marginally to the right of transition point A therefore coalesce as BSs of increasing compactness but not yet as BHs. This effect

also introduces a continuity of  $E_{\text{GW}}(|\phi_c|)$  contrary to the discontinuity expected in the limit of infinite infall time.

**Branch II<sub>UM</sub> (yellow):** Beyond transition point B, on branch II<sub>UM</sub> in Fig. 5, we encounter unstable stars which migrate horizontally to other stable and more compact BS models and eventually merge according to case 3. The transition at B is discontinuous in the sense that the compactness of these equilibrium target configurations differs from that of a BH by a finite amount. We accordingly expect an upward jump in  $E_{\text{GW}}(|\phi_c|)$ . This expectation is fully corroborated in Fig. 1; at  $|\phi_c| = 0.083 M_{\text{Pl}}$ , the GW energy *discontinuously* increases by more than a factor two and a BH only forms post-coalescence (red versus blue dots).

Branch II<sub>UM</sub> is also the home of the “needles”, i.e.  $\mathcal{O}(1)$  relative changes in  $E_{\text{GW}}$  under minuscule variations in  $|\phi_c|$ . We can explain this behavior by recalling the single migrating BS models of Fig. 6. These stars do not complete their migration by quickly settling down into the new equilibrium configuration but rather pulsate around it; cf. the orange curves for  $|\phi_c(t)|$  in the right panels. In a head-on collision of two such stars, this pulsation is abruptly terminated by the merger process. The merger dynamics and consequential GW energy, however, will depend on the momentary phase of the pulsation; do the two stars merge at the moment of maximal expansion or contraction or somewhere in between? It is this pulsation phase and the consequential BS compactness *at merger* that changes by  $\mathcal{O}(1)$  even under a minute change in the initial BSs’ central scalar-field amplitude value  $|\phi_c|$ . The energy  $E_{\text{GW}}$ , as we have already seen, changes accordingly with the BS compactness at merger.

Clearly, since the phase at merger depends on the time of merger, we should expect the structure of the needles to change when we change the initial separation (and hence the infall time). As we will see later in section V D, this is indeed what occurs when we vary the initial separation.

**Branch III:** The transition at point C, where we reach the stable stars of branch III, is continuous in every regard. And yet, point C is special in one important respect: it marks the compactness where the energy function  $E_{\text{GW}}(|\phi_c|)$  must be *extremal*. This can be understood as follows. The branch II<sub>UM</sub> stars located an infinitesimal  $\delta|\phi_c|$  to the left of point C are unstable but migrate horizontally to a new equilibrium configuration also infinitesimally close to point C, just on the right. In consequence, the merger scenarios and, hence, the GW energy values  $E_{\text{GW}}$  of these two slightly different initial configurations must be *identical*; it does not matter whether the stable BS states have been reached through a minor migration or were realized right from the beginning. Thus,  $E_{\text{GW}}$  infinitesimally to the left of point C must equal the value infinitesimally to the right of point C and, hence, must be extremal and smooth at C. Up to minor distortions due to the presence of the needles, we see this behaviour confirmed in Fig. 1 at  $|\phi_c| \approx 0.14$ . As we shall see further below, this remains

<sup>7</sup> Theoretically, they could also coalesce into a more massive BS at merger, but we ubiquitously find them to form a BH.

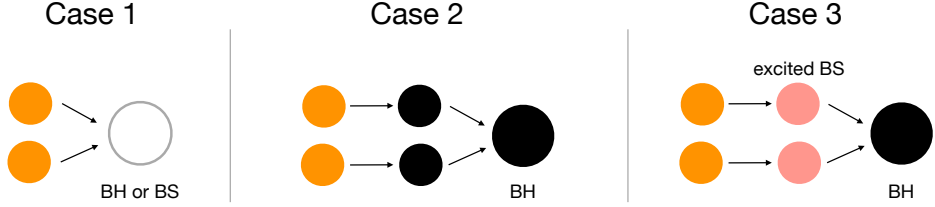


FIG. 7. Illustration of 3 main fates of an equal-mass BS head-on merger encountered in this work. Case A corresponds to initially stable BSs either forming a BH or a BS remnant upon merger, case B to initially unstable BSs collapsing to BHs pre-merger, and case C to initially unstable BSs migrating to excited BS models and continuing their collapse to a BH after merger. We note that in case C we cannot exclude the possibility that a BS remnant is formed post-merger, however, in all of our simulations for this case a BH is formed.

true for other potential functions *provided* transition point C exists and admits stable BS models in its neighbourhood.

**Branch IV:** The transition to branch IV at point D is very similar to that of point A between the stable and unstable branches I and II<sub>UB</sub>. Theoretically we expect the same *discontinuous* jump in the radiated energy back to the BH value  $E_{\text{GW}}^{\text{BH}} \approx 6 \times 10^{-4} M_{\text{tot}}$  and the associated premature BH collapse beyond point D. Unlike point A, our empirical results fully reproduce the theoretical expectations in Fig. 1 at  $|\phi_c| \approx 0.22 M_{\text{Pl}}$ . This excellent agreement directly follows from the generically high BS compactness in this regime; all unstable BSs collapse to BHs rapidly, well within the infall time. Note also that for these configurations there exists no stable BS branch further to the right which might halt or slow down the collapse.

## B. GW Energy dependence on compactness

We now return to the origin of the empirical result that mergers of less compact BS stars are significantly louder than equivalent black hole mergers. To understand this, let us consider the dependence of the GW energy  $E_{\text{GW}}(|\phi_c|)$  as a function of  $|\phi_c|$ , first focusing on the  $\sigma/M_{\text{Pl}} = 0.28725$  models and then generalizing to other potentials.

Starting from the small  $|\phi_c|$  limit of Branch I, as  $|\phi_c| \rightarrow 0$ , we approach the trivial minimum  $V(|\phi_c| \rightarrow 0) = 0$ , so the BS becomes more and more diffuse. Thus we expect in this limit, the GW energy also approaches zero which is manifest in Fig. 1. As we increase  $|\phi_c|$  from this limit and climb the potential, the BS compactness increases, so the GW energy  $E_{\text{GW}}(|\phi_c|)$  also increases. This is an unsurprising consequence of the usual expectation that the GW energy is positively correlated with the compactness. What is surprising however is that by  $|\phi_c| = 0.03 M_{\text{Pl}}$ ,  $E_{\text{GW}}(|\phi_c|)/M_{\text{int}} \approx 0.001$  which is already greater than that of an equivalent BH head one merger with  $E_{\text{GW}}^{\text{BH}} = 0.0006$ , despite the BSs being significantly

less compact.

Obviously, this positive correlation cannot continue indefinitely to higher compactness since eventually one reaches BH compactness. Focusing on Fig. 1, and ignoring for now the messy needles and instabilities that dominate the physics for mid values of  $|\phi_c|$  on Branch II, we see that indeed there exist a turnover at  $|\phi_c| \gtrsim 0.13 M_{\text{Pl}}$  (roughly from the beginning of the stable Branch III) when the transition from positive correlation to negative correlation occurs –  $E_{\text{GW}}(|\phi_c|)$  begins to decrease even as the compactness increases. Finally at  $|\phi_c| = 0.22 M_{\text{Pl}}$ , the GW power discontinuously jumps to the expected GW emission  $E_{\text{GW}}^{\text{BH}} = 0.0006$  from BH collisions – this signals the onset of the case 2 mergers (see Fig. 7) since  $|\phi_c| = 0.22 M_{\text{Pl}}$  is a critical point of BS instability.

Thus we have two seemingly paradoxical results: (a) why should BSs that are less compact than a BH generate more GWs in a merger and (b) why do BSs of very high compactness generate lower GW energy than BSs of low compactness (but still more than BHs)?

For question (a), we have argued in Sec. V A that in a BS merger a greater asymmetry of the coalescence phase generates stronger gravitational radiation. Observation (b) can then be explained by the argument that *higher compactness implies lower deformability*. What we mean by the vague term “deformability” is “the amplitude of the response of the BS system to gravitational and matter perturbations” as quantified through *tidal deformability parameters*; see e.g. Ref. [109]. Since most of the GW emission in a head-on merger is generated during the coalescence phase, it follows that the larger the initial asymmetry of the apparent horizon or compact matter remnant, the higher the GW emission during the merger and ringdown would be. A high compactness, on the other hand, implies a deeper gravitational potential well where matter fields are less susceptible to perturbations during a merger – they are “stiffer”. Clearly, this effect is competing with the fact that systems need to be strongly gravitating before GWs can be produced since spacetime itself is also extremely stiff, hence there is a maximum – in the case of  $\sigma/M_{\text{Pl}} = 0.28725$ , this occurs

at<sup>8</sup>  $|\phi_c| \approx 0.13$  where  $E_{\text{GW}}(|\phi_c|)/M_{\text{tot}} = 0.0035$ .

Finally, we can infer the point of maximal GW emission by recalling that  $E_{\text{GW}}(|\phi_c|)$  is extremal at transition point C connecting branches II and III, provided point C admits stable models in its neighbourhood. Ignoring for the moment the needles and troughs due to premature BH collapse in  $E_{\text{GW}}(|\phi_c|)$ , we can furthermore argue as follows that the extremum is likely to be a maximum: First, we know that  $E_{\text{GW}}(|\phi_c|)$  is a rising function at very small  $|\phi_c|$ .  $E_{\text{GW}}$  can then be minimal at point C only if it has a maximum somewhere between  $|\phi_c| = 0$  and point C. To the left of point C, we would therefore already be in the regime where increasing compactness lowers GW emission. It is hard then to conceive of a physical mechanism that would lead to yet another reversal of  $E_{\text{GW}}(|\phi_c|)$  towards a rising slope. We cannot rigorously rule out that some such mechanism exists, but parsimony suggests the transition point C simply marks the transition from increasing  $E_{\text{GW}}$  (due to increasing compactness) towards decreasing  $E_{\text{GW}}$  (due to reduced asymmetry). Empirically, we find this view fully confirmed; if point C exists and admits stable BSs in its neighbourhood, it marks *maximal* GW emission.

### C. GW energy dependence on $V(\phi)$

Up to this point, we have discussed for the solitonic potential with  $\sigma = 0.28725 M_{\text{Pl}}$  of Fig. 1 all possible features that can arise in the GW emission of BS head-on collisions of different compactness and we have related these features to the types of merger sketched in Fig. 7. The merger cases 1 and 2 will be realized for any potential that admits stable and unstable BSs, but the presence or absence of case 3 will critically depend on the relative location of the two maxima in the  $M(|\phi_c|)$  curve labelled A and D in Fig. 5. Notice from Fig. 4 that both the position and amplitude of the 2nd peak D depend on  $\sigma$  – the larger  $\sigma$ , the larger the  $|\phi_c|$  value of transition point D is while the amplitude of its potential  $V(|\phi_c|)$  becomes smaller. Thus depending on the amplitude of  $\sigma$ , we expect three different possibilities.

- (i) In the mini BS limit where  $\sigma \rightarrow \infty$ , the second peak D occurs at very large compactness, i.e.  $|\phi_c|$  such that all branch III stars are unstable. In this scenario, branches II and III effectively merge with branch IV into one single unstable **UB** branch and the GW energy  $E_{\text{GW}}(|\phi_c|)$  displays a simple behaviour, radiatively efficient BS mergers for small

$|\phi_c|$  and  $E_{\text{GW}}^{\text{BH}} \approx 6 \times 10^{-4} M_{\text{tot}}$  for large  $|\phi_c|$ . This is exactly the behaviour we observe in the top row of Fig. 8 for mini BSs and  $\sigma = 0.5 M_{\text{Pl}}$ .

- (ii) On the other hand, for small  $\sigma/M_{\text{Pl}} \lesssim 0.275$ , the second peak D occurs at sufficiently small  $|\phi_c|$  such that branch III admits stable BSs and the BS mass at point D (significantly) exceeds that of point A. In that case, branch II<sub>UB</sub> is absent. Less compact binaries, i.e. starting to the left of point D, merge according to types 1 or 3 with large  $E_{\text{GW}}$  while merger case 2 is encountered for and only for highly compact binaries starting to the right of point D. In Fig. 8, we encounter this behaviour in the bottom row for  $\sigma = 0.25 M_{\text{Pl}}$ .
- (iii) For moderate values  $0.275 \lesssim \sigma/M_{\text{Pl}} \lesssim 0.4$ , on the other hand, the global maximum of  $M(|\phi_c|)$  is realized at point A (“the first bump is higher”) and then we encounter the entire program of  $E_{\text{GW}}(|\phi_c|)$  as summarized in the previous subsection. This is the case displayed in Fig. 1 for  $\sigma = 0.28725 M_{\text{Pl}}$  and in the center row of Fig. 8 for  $\sigma = 0.3 M_{\text{Pl}}$ .

Results for further values of the solitonic potential parameter  $\sigma$  are presented in Ref. [82]; all of these fall into one of the three regimes listed here.

The remarkably rich structure that we have encountered in the dependence of the GW energy on the BS parameters is not accompanied by a corresponding complexity in the GW signals. Rather, we universally observe rather standard head-on waveforms with a shape quite indistinguishable by eye from their BH counterparts. For example, we display in Fig. 9 the leading quadrupole mode of the Newman-Penrose scalar  $\Psi_4$  for  $\sigma = 0.25 M_{\text{Pl}}$  and various scalar-field amplitudes including configurations of the needle regime. All signals have the overall structure, also seen for BHs, as for example in Fig. 8 of Ref. [111], and only differ significantly in their overall amplitude.

### D. Impact of the initial BS separation

In our discussion in section V A, we have identified two features in the shape of the GW energy  $E_{\text{GW}}(|\phi_c|)$  which we expect to vary with the initial separation of the binary. The first observation concerns BS mergers with correspondingly large GW emission on the *early* part of branch II<sub>UB</sub> to the right of transition point A, despite the fact that they are unstable to BH collapse. How can this be? The answer lies in the inevitably finite infall time of our BS collisions; in Fig. 6, the left, third from top panel demonstrates that for  $\sigma = 0.28725$  and  $|\phi_c| \lesssim 0.06 M_{\text{Pl}}$ , BSs are indeed unstable to BH collapse but take a long time to do so, longer, in fact, than the duration of their infall. They consequently merge as increasingly compact BSs but not yet as BHs. At  $|\phi_c| = 0.068 M_{\text{Pl}}$  we finally reach BSs so unstable that they complete their individual collapse prior to encountering each other. This behaviour

<sup>8</sup> It has been argued in Ref. [110] that in the strong-field regime, non-linearities around merger are rapidly encompassed by a common horizon (see their Sec. II B) and thus will not reach a detector outside the event horizon. Our observation of enhanced GW energy from more asymmetric mergers is independent of this interpretation of captured non-linearities.

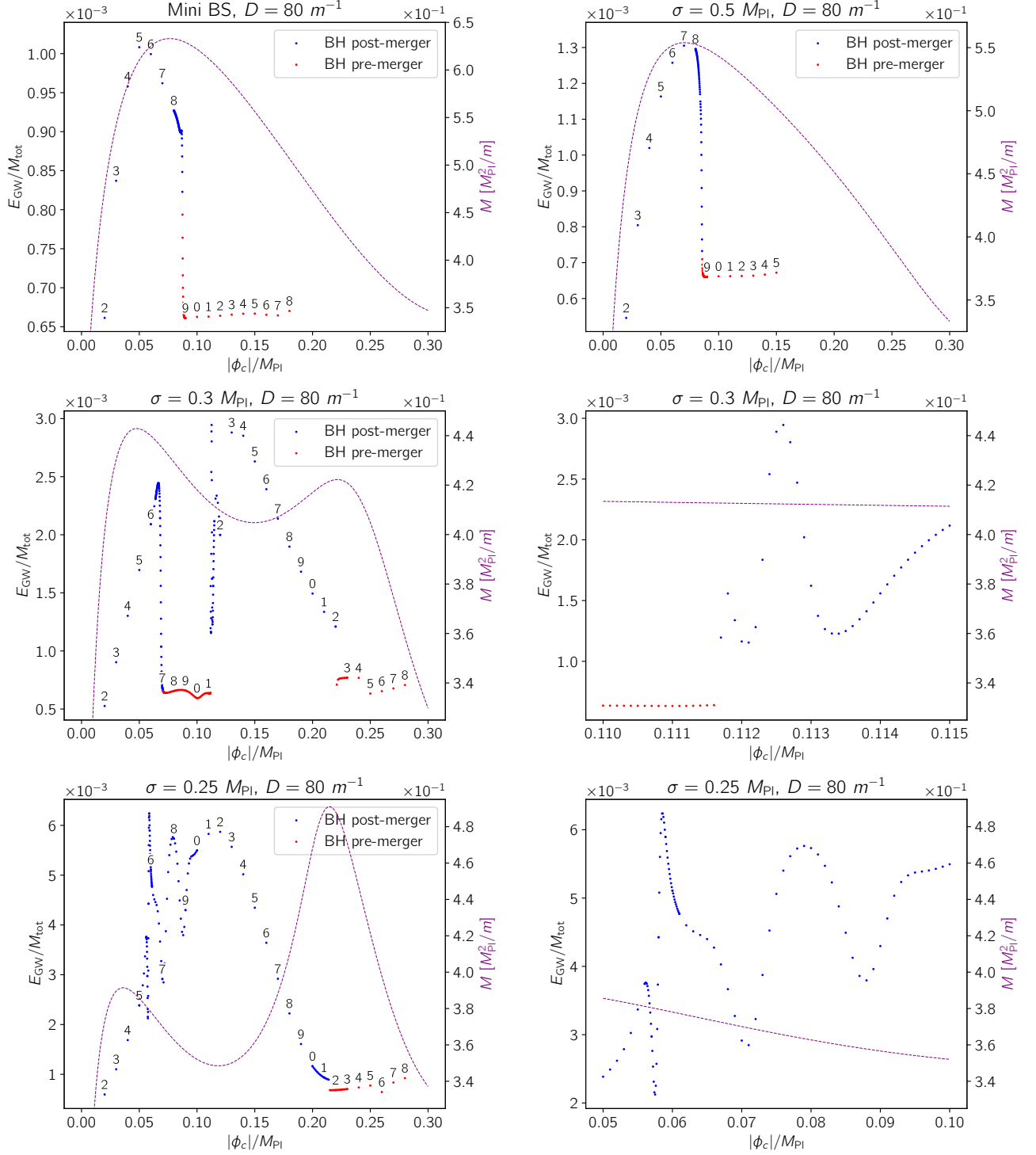


FIG. 8. As in Fig. 1 but for different scalar potentials  $V(|\phi_c|)$ , this figure shows the GW energy released in equal-mass BS head-on collisions as a function of the individual BSs' central scalar-field amplitude  $|\phi_c|$ . Here, red dots denote configurations where the individual BSs collapse into BHs prior to coalescence and blue symbols represent binaries where the constituents retain their BS character up to merger upon which they form a single BH or BS remnant. For reference, we also display in each panel by the dashed purple curve the  $M(|\phi_c|)$ , i.e. mass vs. scalar amplitude, curve of the corresponding equilibrium BS models. Note that the center- and bottom-right panels are zoom-in versions of the respective left panels.

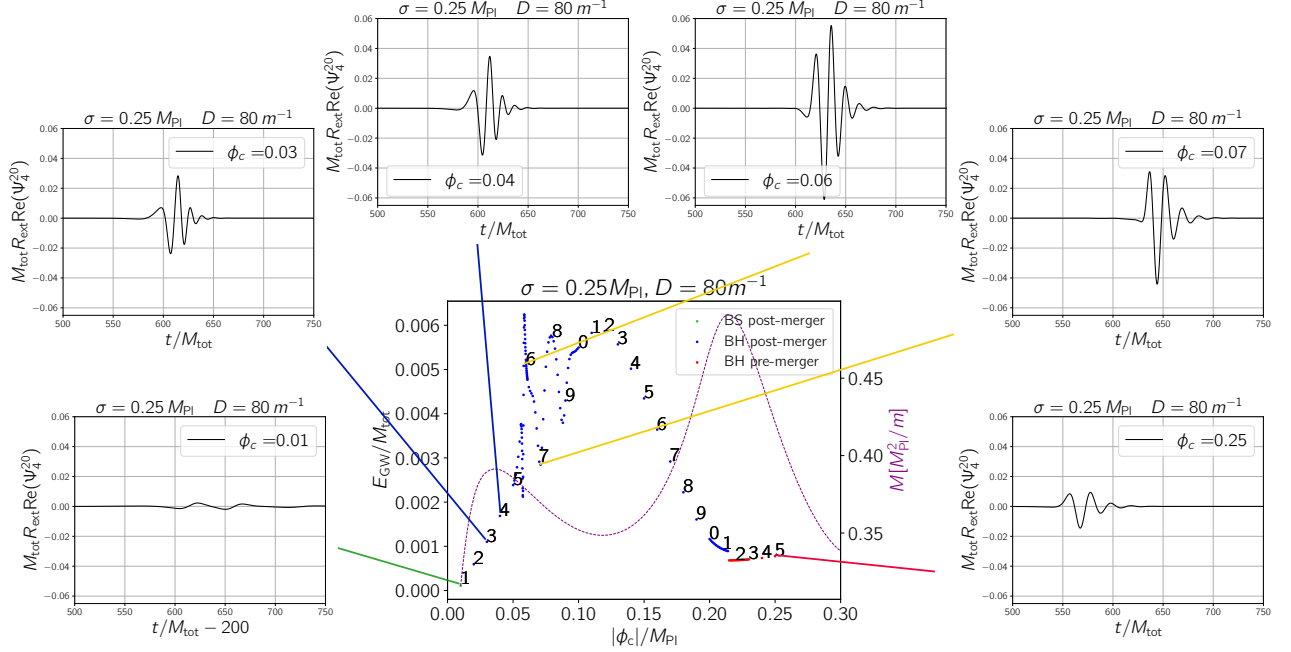


FIG. 9. The GW signals from selected BS collisions for  $\sigma = 0.25 M_{\text{Pl}}$  are shown in the form of the dominant quadrupole contribution of the Newman-Penrose scalar  $\Psi_4$ . The straight lines, color coded according to the branch colors of Fig. 5, connect the individual waveforms to the corresponding configuration in the  $E_{\text{GW}}(|\phi_c|)$  curve. The signals exhibit a wide range of amplitudes, in accordance with the GW energy values of the central panel, but all agree quite closely in their overall shape. Note that for the green line ( $|\phi_c| = 0.01 M_{\text{Pl}}$  merger) is that of Case 1 (merger into another BS).

also explains the continuity of the curve  $E_{\text{GW}}(|\phi_c|)$  curve at  $|\phi_c| = 0.068 M_{\text{Pl}}$  in Fig. 1; for each finite infall time, we can fine tune  $|\phi_c|$  to obtain any “desired” BS compactness at merger – note that these BSs are *not* in equilibrium and, hence, not constrained by the maximum compactness of equilibrium stars. We have tested this hypothesis by rerunning selected configurations in this regime with different initial separation  $D$  but all other parameters unchanged. We indeed find in these simulations that the sharp drop in the GW energy towards  $E_{\text{GW}}^{\text{BH}}$  moves towards larger  $|\phi_c|$  when we decrease  $D$  whereas it converges to the transition point A in the limit  $D \rightarrow \infty$ .

The second feature is the structure of the needles under variations in the initial separation; here a different infall time implies a different cut-off of the migrating BSs’ radial pulsations. The structure of the needles in the  $E_{\text{GW}}(|\phi_c|)$  curve should then change when varying  $D$ . We verify this interpretation in Fig. 10 where we plot the GW energy for  $\sigma = 0.25 M_{\text{Pl}}$  but now with initial binary separation  $D = 60 m^{-1}$ . Our expectation is fully borne out by comparing this figure with the analogous results for  $D = 80 m^{-1}$  in the bottom left panel of Fig. 8; the needles have drastically different shape while  $E_{\text{GW}}^{\text{BH}}$  retains its overall shape in every other regard.

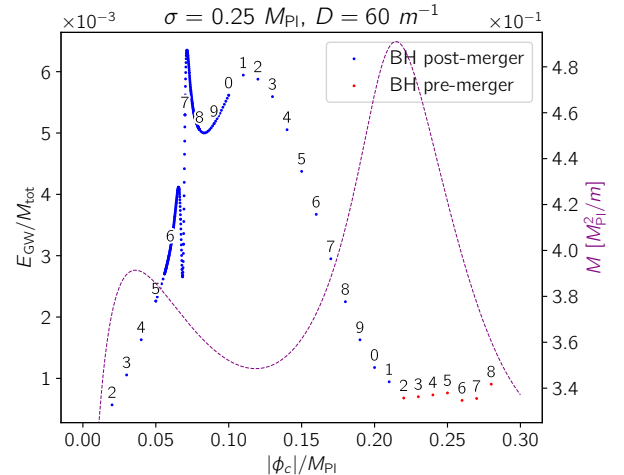


FIG. 10. As Fig. 8 but for  $\sigma = 0.25 M_{\text{Pl}}$  and a smaller initial binary separation  $D = 60 m^{-1}$ . Compared to the bottom left panel of Fig. 8, we see that the different initial separation significantly changes the structure of the needles in  $E_{\text{GW}}(|\phi_c|)$  around  $|\phi_c| = 0.07 M_{\text{Pl}}$  but leaves the curve virtually unaltered everywhere else.

## VI. DISCUSSION

In this work, we have undertaken an exhaustive numerical and theoretical investigation of the physics of GW production in head-on boson stars mergers, scanning over both the parameter space  $\sigma$  of the solitonic potential and compactness parametrized by the central scalar amplitude  $|\phi_c|$  for equilibrium BS solutions. While we have summarised the results in the introduction section I, it is worth asking which of the results discussed are model specific to the solitonic model we have studied and which are general broad lessons applicable to other models.

The most striking result is the fact that BS mergers at high compactness generate more gravitational radiation than equivalent mergers of BHs. This was first noted in studies of solitonic models in Refs. [44, 52] and in Ref. [65] for the  $m^2\phi^2$  model of a real scalar field (sometimes called an *oscillaton*). The fact that it appears in both real and complex scalar models suggests that *head-on mergers of compact bosonic self-gravitating stars generate significantly more GW energy than equivalent BH mergers*. It is thus an interesting question to ask whether this result extends to inspiral mergers of BSs. Indeed, our results demonstrate that, above some model-dependent compactness, BS mergers are *always* louder than BHs, even if they eventually approach (but do not reach) BH compactness – “deformable BSs are louder than stiff BHs”. Our conjecture for this result – supported by the numerical observations of “needles” in the GW power during mergers of unstable Branch IIUM mergers – is that during the collision phase, the increased deformation in a less compact BS results in a more strongly perturbed and asymmetric merger remnant whose subsequent relaxation generates more GWs. *It will be interesting to see if this result extends to other types of horizonless compact objects such as Proca stars or perhaps even NSs.*

In general, BS models become unstable at high (but below BH) compactness where perturbations can trigger a rapid collapse to a BH. In both mini-BS and oscillaton models, this represents the only delineation point between stable and unstable BSs. However, in more complicated models with two or more minima in the potential, the presence of additional stable and unstable equilibrium points in the potential  $V(|\phi_c|)$  can introduce additional structure in the stability diagram (see e.g. Ref. [112]). For the solitonic models we have studied, this manifests itself in the form of additional stable/unstable branches in the solution space of BSs (see Fig. 4). In these additional unstable regions, a BS may either collapse to a BH or migrate to a different BS. In all cases, the existence of these unstable regions implies that, in the limit of infinite infall time, *the GW energy  $E_{\text{GW}}(|\phi_c|)$  is discontinuous at the points of transition from stable to unstable branches*. Unfortunately, since we do not measure GW energies over extraction spheres directly, but only the strain at one point on the sphere,

there is scant hope for observing such discontinuities.

In section IV, we have studied in detail the nature of the instability, in particular the time-scale or *migration time* of the transition. Furthermore, if the instability leads to a transition into another (excited) BS which oscillates, then we should expect “needles” structure in the energy function  $E_{\text{GW}}(|\phi_c|)$ . The main lesson here is that, *there can be rapid changes in GW energy over small changes in the parameter space*. For example, if we merge two equal mass oscillating BSs, the GW emitted would depend strongly on the *phase* of the pulsation at merger, complicating any observational inference over its progenitors. This raises two further important questions. (i) *What is the timescale of relaxation of dynamic BS configurations to an equilibrium state?* Numerical studies often result in long-lived dynamical stars (see e.g. Refs. [45, 72] or our Fig. 5), but is it long enough to be of relevance for inspirals? (ii) *What kind of environmental effects could induce dynamic perturbations of the kind experienced by our unstable migrating BSs?*

One important point we would like to emphasise is that this work is focused on the mergers of *in-phase* BSs. However, as first investigated in [50], it is well known that *off-phase* BSs exhibit significant deviation in the merger dynamics from in-phase BS. Broadly speaking, BSs with different phases exhibit *repulsive* forces with the magnitude depending on how off-phase they are [52] – this is due to the fact that BSs are wave-like objects and can interfere either constructively or destructively depending on their phases. It is unclear at the moment how these interference effects will affect mergers of unstable or near-unstable BSs. As a guess to one of its possible effects in BSs, we note that in off-phase mergers of real scalar Oscillatons [67], it was shown that while off-phase repulsion resists the formation of BHs from direct mergers, the subsequent “compression” of *individual* Oscillatons due to the repulsion can cause sufficiently large disruption such that it collapses into a BH on its own. Thus, applying this logic to each BS, we anticipate that this might lead to a widening of the “red dots band” say in Fig. 1, although clearly there is plenty of scope for further investigation in this direction. Also, examining how waveforms change with the self-interaction parameter would provide a more complete perspective, and we leave this for future work.

Finally, any program to search for BSs in the observational data stream requires the construction of waveform models or templates akin to the `IMRPhenom`, `SEOBNR` or `NRSur` approximants for BH-binary mergers. Our results suggest that the GWs from the BS star merger phase can exhibit significant differences in the GW amplitude as compared to BH mergers; cf. Fig. 9. The GW amplitude, however, is essentially degenerate with the luminosity distance and thus of little help for characterizing the nature of the source. This naturally raises the question *whether the GW signature of the needle regime may exhibit more structural features in inspirals and/or for other BS parameters like unequal mass ratios or non-zero*

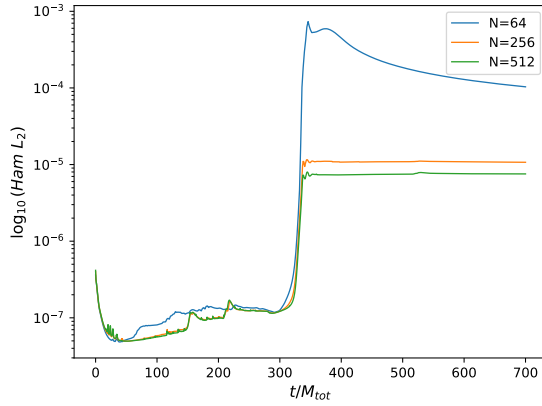


FIG. 11. The  $L_2$  norm of the Hamiltonian constraint as a function of time obtained for the BS binary configuration  $\sigma_0 = 0.25$ ,  $|\phi_c| = 0.02$  using different resolutions  $N = 64$ ,  $N = 256$  and  $N = 1024$ .

spins. Depending on the longevity of BS perturbations, comprehensive binary BS templates may need to account for these effects, perhaps using phenomenological parameters to extend simple semi-analytic quadrupole models (e.g. Ref. [113]) with rigid mass distributions. Given the complexity of the merger physics, however, we suspect that surrogate models, as for example constructed for Proca-star head-on mergers in Ref [74], may provide the most efficient way forward.

## ACKNOWLEDGMENTS

This work has been supported by. STFC Research Grant No. ST/V005669/1, NSF Grant Nos. PHY-1626190 and PHY-2110594, and ExCALIBUR Hardware and Enabling Software Grant Nos. ST/X001393/1 and EP/Y028082/1. We acknowledge support by the Cambridge Service for Data Driven Discovery at the University of Cambridge and Durham University through DiRAC Projects ACTP284 and ACTP and STFC capital Grants No. ST/P002307/1 and No. ST/R002452/1, and STFC operations Grant No. ST/R00689X/1. We acknowledge support by the Texas Advanced Computing Center (TACC) and the San Diego Supercomputing Center (SDSC) through NSF Grant No. PHY-090003. Computations were done on the CSD3 and Fawcett (Cambridge), Cosma7 and 8 (Durham), Stampede2 and Stampede3 (TACC), and Expanse (SDSC) clusters. EL and BG acknowledge computations resources provided by a DiRAC RAC15 grant ACTP316. RC and TE have been supported by the Centre for Doctoral Training (CDT) at the University of Cambridge funded through STFC. TE acknowledges Perimeter Institute for Theoretical Physics, supported by the Government of Canada through the Department of Innovation, Science and Economic Development and by the Province of Ontario through the Ministry of Colleges and Universities

## Appendix A: Constraint violations

The constraint violations observed in our simulations follow the pattern exemplified for the Hamiltonian constraint  $H$  of the BS collision with parameters  $\sigma = 0.25$ ,  $|\phi_c| = 0.02$  in Fig. 11. At early times, the constraint damping of the CCZ4 formulation reduces the constraint violations by an order of magnitude independent of numerical resolution. During the remainder of the infall, up to about  $t = 300 M$ , the constraint violations of the  $N = 256$  and  $N = 512$  simulations nearly overlap. We attribute this to the fact that the constraint violations have very low magnitude and are initial-data dominated. To test this hypothesis, we have added a third simulation with lower resolution  $N = 64$ . This indeed exhibits a significant contribution to  $H$  arising from the discretization error with convergence of about second order. During merger, the constraint violations increase substantially, as expected for the formation of the extreme curvature region of a black hole<sup>9</sup>. Post merger, we observe convergence between first and second order.

## Appendix B: Gravitational Wave Extraction

Numerical relativity simulations in  $3 + 1$  dimensions commonly use the Newman-Penrose scalar  $\Psi_4$  to extract gravitational radiation. Here we follow the discussion of GW extraction in  $d + 1$  dimensions of Ref. [114] and apply it to our case of  $2 + 1$  evolutions ( $d = 2$ ). The outgoing gravitational radiation is encoded in the the projections of the Weyl tensor  $C_{ABCD}$  onto a null tetrad  $\{k^A, l^A, m^A, \bar{m}^A\}$

$$\Psi_4 = C_{ABCD} k^A \bar{m}^B k^C \bar{m}^D; \quad (B1)$$

here capital Latin indices run from 0 to  $d$ . In order to construct the null tetrad, we first define an orthonormal basis  $\{e_{(0)}^A, e_{(1)}^A, e_{(2)}^A, e_{(3)}^A\}$ , where  $e_{(0)}^A$  is the unit normal to the spatial hypersurfaces,  $e_{(1)}^A$  is the unit normal radial vector and  $e_{(2)}^A, e_{(3)}^A$  are the angular vectors, which are typically constructed via Gram-Schmidt orthonormalisation. We then pick the tetrad consisting of ingoing and outgoing null vectors,  $k^A$  and  $l^A$  respectively, and a com-

<sup>9</sup> Note that this effect is enhanced by the effectively two-dimensional domain, which for purely geometric reasons attaches relatively higher weight to grid points near the black hole as compared to a three-dimensional grid.

plex null vector  $m^A$  and its conjugate  $\bar{m}^A$ ,

$$l^A = \frac{1}{\sqrt{2}} \left( e_{(0)}^A + e_{(1)}^A \right), \quad (B2)$$

$$k^A = \frac{1}{\sqrt{2}} \left( e_{(0)}^A - e_{(1)}^A \right), \quad (B3)$$

$$m^A = \frac{1}{\sqrt{2}} \left( e_{(2)}^A + ie_{(3)}^A \right), \quad (B4)$$

$$\bar{m}^A = \frac{1}{\sqrt{2}} \left( e_{(2)}^A - ie_{(3)}^A \right). \quad (B5)$$

Following the notation of Ref. [114], we will denote the off-domain components with a 'w' index, so that in  $2+1$  we have,  $e_{(3)}^A \rightarrow e_{(w)}^A$ . It is then straightforward to show that the outgoing gravitational radiation in Eq. (B1) can be re-expressed by the real quantity

$$\begin{aligned} \Omega_{(a)(b)} = & \frac{1}{4} (R_{0B0D} e_{(a)}^B e_{(b)}^D - R_{AB0D} e_{(1)}^A e_{(a)}^B e_{(b)}^D \\ & - R_{0BCDE} e_{(a)}^B e_{(b)}^D e_{(1)}^C + R_{ABCDE} e_{(1)}^A e_{(a)}^B e_{(b)}^D e_{(1)}^C), \end{aligned} \quad (B6)$$

where we have introduced early lower-case Latin indices  $a, b, \dots$  to span the angular directions (i.e. 2 and 3) and used the fact that the GW signal is calculated in vacuum, where the Weyl and Riemann tensors are the same. Therefore different  $(a, b)$  indices correspond to different polarisation content. A direct calculation results in the following relationship between  $\Omega_{(a)(b)}$  and  $\Psi_4$  in  $2+1$  dimensions,

$$\text{Re}(\Psi_4) = \Omega_{22} - \Omega_{ww} \quad (B7)$$

$$\text{Im}(\Psi_4) = -2\Omega_{2w} = 0, \quad (B8)$$

where  $\Omega_{22}$  and  $\Omega_{ww}$  can be obtained directly from Eqs.(4.22)-(4.35) of Ref. [114].

---

[1] A. Hewish, S. J. Bell, J. D. H. Pilkington, P. F. Scott, and R. A. Collins, *Nature* **217**, 709 (1968).

[2] S. L. Shapiro and S. A. Teukolsky, *Black Holes, White Dwarfs, and Neutron Stars* (John Wiley & Sons, Inc., 1983).

[3] E. Berger, *Ann. Rev. Astron. Astrophys.* **52**, 43 (2014), arXiv:1311.2603 [astro-ph.HE].

[4] B. P. Abbott *et al.* (LIGO Scientific, Virgo, Fermi GBM, INTEGRAL, IceCube, AstroSat Cadmium Zinc Telluride Imager Team, IPN, Insight-Hxmt, ANTARES, Swift, AGILE Team, 1M2H Team, Dark Energy Camera GW-EM, DES, DLT40, GRAWITA, Fermi-LAT, ATCA, ASKAP, Las Cumbres Observatory Group, OzGrav, DWF (Deeper Wider Faster Program), AST3, CAASTRO, VINROUGE, MASTER, J-GEM, GROWTH, JAGWAR, CaltechNRAO, TTU-NRAO, NuSTAR, Pan-STARRS, MAXI Team, TZAC Consortium, KU, Nordic Optical Telescope, ePESSTO, GROND, Texas Tech University, SALT Group, TOROS, BOOTES, MWA, CALET, IKI-GW Follow-up, H.E.S.S., LOFAR, LWA, HAWC, Pierre Auger, ALMA, Euro VLBI Team, Pi of Sky, Chandra Team at McGill University, DFN, ATLAS Telescopes, High Time Resolution Universe Survey, RIMAS, RATIR, SKA South Africa/MeerKAT), *Astrophys. J. Lett.* **848**, L12 (2017), arXiv:1710.05833 [astro-ph.HE].

[5] A. Cattaneo *et al.*, *Nature* **460**, 213 (2009), arXiv:0907.1608 [astro-ph.CO].

[6] M. J. Rees, *Ann. Rev. Astron. Astrophys.* **22**, 471 (1984).

[7] P. Reig, *Astrophys. Space Sci.* **332**, 1 (2011), arXiv:1101.5036 [astro-ph.HE].

[8] A. Escrivà, F. Kuhnel, and Y. Tada, (2022), arXiv:2211.05767 [astro-ph.CO].

[9] F. Özel and P. Freire, *Ann. Rev. Astron. Astrophys.* **54**, 401 (2016), arXiv:1603.02698 [astro-ph.HE].

[10] B. P. Abbott *et al.* (LIGO Scientific, Virgo), *Phys. Rev. Lett.* **121**, 161101 (2018), arXiv:1805.11581 [gr-qc].

[11] J. M. Lattimer, *Ann. Rev. Nucl. Part. Sci.* **71**, 433 (2021).

[12] V. Cardoso, L. Gualtieri, C. Herdeiro, and U. Sperhake, *Living Rev. Relativity* **18**, 1 (2015), arXiv:1409.0014 [gr-qc].

[13] L. Barack *et al.*, *Class. Quant. Grav.* **36**, 143001 (2019), arXiv:1806.05195 [gr-qc].

[14] V. Cardoso, O. J. C. Dias, G. S. Hartnett, M. Middleton, P. Pani, and J. E. Santos, *JCAP* **1803**, 043 (2018), arXiv:1801.01420 [gr-qc].

[15] E. Berti *et al.*, *Class. Quant. Grav.* **32**, 243001 (2015), arXiv:1501.07274 [gr-qc].

[16] R. Abbott *et al.* (LIGO Scientific, VIRGO, KAGRA), (2021), arXiv:2112.06861 [gr-qc].

[17] B. P. Abbott *et al.*, *Phys. Rev. Lett.* **116**, 061102 (2016), arXiv:1602.03837 [gr-qc].

[18] R. Abbott *et al.* (KAGRA, VIRGO, LIGO Scientific), *Phys. Rev. X* **13**, 041039 (2023), arXiv:2111.03606 [gr-qc].

[19] J. L. Feng, *Ann. Rev. Astron. Astrophys.* **48**, 495 (2010), arXiv:1003.0904 [astro-ph].

[20] F. Kahlhoefer, *Int. J. Mod. Phys. A* **32**, 1730006 (2017), arXiv:1702.02430 [hep-ph].

[21] S. Cebrián, *J. Phys. Conf. Ser.* **2502**, 012004 (2023), arXiv:2205.06833 [physics.ins-det].

[22] P. Jaranowski and A. Krolak, *Living Rev. Rel.* **8**, 3 (2005), arXiv:0711.1115 [gr-qc].

[23] M. Maggiore, *Gravitational Waves. Vol. 1: Theory and Experiments*, Oxford Master Series in Physics (Oxford University Press, 2007).

[24] T. Evstafyeva, U. Sperhake, I. Romero-Shaw, and M. Agathos, (2024), arXiv:2406.02715 [gr-qc], arXiv:2406.02715 [gr-qc].

[25] S. L. Liebling and C. Palenzuela, *Living Rev. Rel.* **15**, 6 (2012), arXiv:1202.5809 [gr-qc].

[26] L. Visinelli, *Int. J. Mod. Phys. D* **30**, 2130006 (2021), arXiv:2109.05481 [gr-qc].

[27] M. Bezares and N. Sanchis-Gual, (2024), arXiv:2406.04901 [gr-qc].

[28] J. C. Aurrekoetxea, C. Hoy, and M. Hannam, *Phys. Rev. Lett.* **132**, 181401 (2024), arXiv:2312.03860 [gr-qc].

[29] J. Calderón Bustillo, N. Sanchis-Gual, A. Torres-Forné, J. A. Font, A. Vajpeyi, R. Smith, C. Herdeiro, E. Radu, and S. H. W. Leong, *Phys. Rev. Lett.* **126**, 081101 (2021), arXiv:2009.05376 [gr-qc].

[30] D. J. Kaup, *Phys. Rev.* **172**, 1331 (1968).

[31] N. Siemonse and W. E. East, *Phys. Rev. D* **103**, 044022 (2021), arXiv:2011.08247 [gr-qc].

[32] N. Sanchis-Gual, F. Di Giovanni, M. Zilhão, C. Herdeiro, P. Cerdá-Durán, J. A. Font, and E. Radu, *Phys. Rev. Lett.* **123**, 221101 (2019), arXiv:1907.12565 [gr-qc].

[33] S. Yoshida and Y. Eriguchi, *Phys. Rev. D* **56**, 762 (1997).

[34] E. W. Mielke, *Fundam. Theor. Phys.* **183**, 115 (2016).

[35] B. Kleihaus, J. Kunz, and M. List, *Phys. Rev. D* **72**, 064002 (2005), arXiv:gr-qc/0505143.

[36] F. Di Giovanni, N. Sanchis-Gual, P. Cerdá-Durán, M. Zilhão, C. Herdeiro, J. A. Font, and E. Radu, *Phys. Rev. D* **102**, 124009 (2020), arXiv:2010.05845 [gr-qc].

[37] A. S. Dmitriev, D. G. Levkov, A. G. Panin, E. K. Pushnaya, and I. I. Tkachev, *Phys. Rev. D* **104**, 023504 (2021), arXiv:2104.00962 [gr-qc].

[38] V. Cardoso, P. Pani, M. Cadoni, and M. Cavaglia, *Phys. Rev. D* **77**, 124044 (2008), arXiv:0709.0532 [gr-qc].

[39] C.-W. Lai, *A Numerical study of boson stars*, Other thesis (2004), arXiv:gr-qc/0410040.

[40] N. Siemonse, *Phys. Rev. Lett.* **133**, 031401 (2024), arXiv:2404.14536 [gr-qc].

[41] P. V. P. Cunha, E. Berti, and C. A. R. Herdeiro, *Phys. Rev. Lett.* **119**, 251102 (2017), arXiv:1708.04211 [gr-qc].

[42] V. Cardoso, E. Franzin, and P. Pani, *Phys. Rev. Lett.* **116**, 171101 (2016), [Erratum: *Phys. Rev. Lett.* 117,no.8,089902(2016)], arXiv:1602.07309 [gr-qc].

[43] P. V. P. Cunha, C. Herdeiro, E. Radu, and N. Sanchis-Gual, *Phys. Rev. Lett.* **130**, 061401 (2023), arXiv:2207.13713 [gr-qc].

[44] T. Helfer, U. Sperhake, R. Croft, M. Radia, B.-X. Ge, and E. A. Lim, *Class. Quant. Grav.* **39**, 074001 (2022), arXiv:2108.11995 [gr-qc].

[45] R. Croft, T. Helfer, B.-X. Ge, M. Radia, T. Evstafyeva, E. A. Lim, U. Sperhake, and K. Clough, *Class. Quant. Grav.* **40**, 065001 (2023), arXiv:2207.05690 [gr-qc].

[46] C. Palenzuela, P. Pani, M. Bezares, V. Cardoso, L. Lehner, and S. Liebling, *Phys. Rev. D* **96**, 104058 (2017), arXiv:1710.09432 [gr-qc].

[47] F. Atteneder, H. R. Rüter, D. Cors, R. Rosca-Mead, D. Hilditch, and B. Brügmann, *Phys. Rev. D* **109**, 044058 (2024), arXiv:2311.16251 [gr-qc].

[48] M. Bezares, C. Palenzuela, and C. Bona, *Phys. Rev. D* **95**, 124005 (2017), arXiv:1705.01071 [gr-qc].

[49] N. Sanchis-Gual, M. Zilhão, C. Herdeiro, F. Di Giovanni, J. A. Font, and E. Radu, *Phys. Rev. D* **102**, 101504 (2020), arXiv:2007.11584 [gr-qc].

[50] C. Palenzuela, L. Lehner, and S. L. Liebling, *Phys. Rev. D* **77**, 044036 (2008), arXiv:0706.2435 [gr-qc].

[51] B. C. Mundim, *A Numerical Study of Boson Star Binaries*, Ph.D. thesis, British Columbia U. (2010), arXiv:1003.0239 [gr-qc].

[52] T. Evstafyeva, U. Sperhake, T. Helfer, R. Croft, M. Radia, B.-X. Ge, and E. A. Lim, *Class. Quant. Grav.* **40**, 085009 (2023), arXiv:2212.08023 [gr-qc].

[53] N. Siemonse and W. E. East, *Phys. Rev. D* **108**, 124015 (2023), arXiv:2306.17265 [gr-qc].

[54] M. Bezares, M. Bošković, S. Liebling, C. Palenzuela, P. Pani, and E. Barausse, *Phys. Rev. D* **105**, 064067 (2022), arXiv:2201.06113 [gr-qc].

[55] T. Dietrich, S. Ossokine, and K. Clough, *Class. Quant. Grav.* **36**, 025002 (2019), arXiv:1807.06959 [gr-qc].

[56] K. Clough, T. Dietrich, and J. C. Niemeyer, *Phys. Rev. D* **98**, 083020 (2018), arXiv:1808.04668 [gr-qc].

[57] V. Cardoso, T. Ikeda, Z. Zhong, and M. Zilhão, *Phys. Rev. D* **106**, 044030 (2022), arXiv:2206.00021 [gr-qc].

[58] M. Bezares and C. Palenzuela, *Class. Quant. Grav.* **35**, 234002 (2018), arXiv:1808.10732 [gr-qc].

[59] M. Alcubierre, J. Barranco, A. Bernal, J. C. Degollado, A. Diez-Tejedor, M. Megevand, D. Nunez, and O. Sarbach, *Class. Quant. Grav.* **35**, 19LT01 (2018), arXiv:1805.11488 [gr-qc].

[60] N. Sanchis-Gual, F. Di Giovanni, C. Herdeiro, E. Radu, and J. A. Font, *Phys. Rev. Lett.* **126**, 241105 (2021), arXiv:2103.12136 [gr-qc].

[61] V. Jaramillo, N. Sanchis-Gual, J. Barranco, A. Bernal, J. C. Degollado, C. Herdeiro, and D. Núñez, *Phys. Rev. D* **101**, 124020 (2020), arXiv:2004.08459 [gr-qc].

[62] A. Bernal, J. Barranco, D. Alic, and C. Palenzuela, *Phys. Rev. D* **81**, 044031 (2010), arXiv:0908.2435 [gr-qc].

[63] S. H. Hawley and M. W. Choptuik, *Phys. Rev. D* **67**, 024010 (2003), arXiv:gr-qc/0208078.

[64] F. S. Guzmán and A. A. Avilez, *Phys. Rev. D* **97**, 116003 (2018), arXiv:1804.08670 [gr-qc].

[65] T. Helfer, E. A. Lim, M. A. G. Garcia, and M. A. Amin, *Phys. Rev. D* **99**, 044046 (2019), arXiv:1802.06733 [gr-qc].

[66] R. Brito, V. Cardoso, C. F. B. Macedo, H. Okawa, and C. Palenzuela, *Phys. Rev. D* **93**, 044045 (2016), arXiv:1512.00466 [astro-ph.SR].

[67] J. Y. Widdicombe, T. Helfer, and E. A. Lim, *JCAP* **2001**, 027 (2020), arXiv:1910.01950 [astro-ph.CO].

[68] P. Grandclement, G. Fodor, and P. Forgacs, *Phys. Rev. D* **84**, 065037 (2011), arXiv:1107.2791 [gr-qc].

[69] R. Brito, V. Cardoso, C. A. R. Herdeiro, and E. Radu, *Phys. Lett.* **B752**, 291 (2016), arXiv:1508.05395 [gr-qc].

[70] N. Sanchis-Gual, C. Herdeiro, J. A. Font, E. Radu, and F. Di Giovanni, *Phys. Rev. D* **99**, 024017 (2019), arXiv:1806.07779 [gr-qc].

[71] C. A. R. Herdeiro, E. Radu, N. Sanchis-Gual, N. M. Santos, and E. dos Santos Costa Filho, *Phys. Lett. B* **852**, 138595 (2024), arXiv:2311.14800 [gr-qc].

[72] N. Siemonse and W. E. East, *Phys. Rev. D* **107**, 124018 (2023), arXiv:2302.06627 [gr-qc].

[73] J. Y. Widdicombe, T. Helfer, D. J. E. Marsh, and E. A. Lim, *JCAP* **10**, 005 (2018), arXiv:1806.09367 [astro-ph.CO].

[74] R. Luna, M. Llorens-Monteagudo, A. Lorenzo-Medina, J. Calderón Bustillo, N. Sanchis-Gual, A. Torres-Forné,

J. A. Font, C. A. R. Herdeiro, and E. Radu, (2024), arXiv:2404.01395 [gr-qc].

[75] C. Palenzuela, I. Olabarrieta, L. Lehner, and S. L. Liebling, Phys. Rev. D **75**, 064005 (2007), gr-qc/0612067.

[76] D. I. Choi, K. C. W. Lai, M. W. Choptuik, E. W. Hirschmann, S. L. Liebling, and F. Pretorius (2009).

[77] M. W. Choptuik and F. Pretorius, Phys. Rev. Lett. **104**, 111101 (2010), arXiv:0908.1780 [gr-qc].

[78] K. Thorne, in *Magic Without Magic*, edited by J. Klauder (Freeman, San Francisco, 1972) p. 231.

[79] N. Sanchis-Gual, J. Calderón Bustillo, C. Herdeiro, E. Radu, J. A. Font, S. H. W. Leong, and A. Torres-Forné, Phys. Rev. D **106**, 124011 (2022), arXiv:2208.11717 [gr-qc].

[80] U. Sperhake, W. Cook, and D. Wang, Phys. Rev. D **100**, 104046 (2020), 1909.02997.

[81] T. Evstafyeva, R. Rosca-Mead, U. Sperhake, and B. Bruegmann, Phys. Rev. D **108**, 104064 (2023), arXiv:2310.05200 [gr-qc].

[82] B.-X. Ge, *Gravitational Waves in Boson Star Mergers*, Doctoral thesis, King's College London (2024).

[83] K. Clough, P. Figueras, H. Finkel, M. Kunesch, E. A. Lim, and S. Tunyasuvunakool, Class. Quant. Grav. **32**, 245011 (2015), arXiv:1503.03436 [gr-qc].

[84] M. Radia, U. Sperhake, A. Drew, K. Clough, P. Figueras, E. A. Lim, J. L. Ripley, J. C. Aurrekoetxea, T. França, and T. Helfer, Class. Quant. Grav. **39**, 135006 (2022), arXiv:2112.10567 [gr-qc].

[85] T. Andrade *et al.*, J. Open Source Softw. **6**, 3703 (2021), arXiv:2201.03458 [gr-qc].

[86] D. Alic, C. Bona-Casas, C. Bona, L. Rezzolla, and C. Palenzuela, Phys. Rev. D **85**, 064040 (2012), arXiv:1106.2254 [gr-qc].

[87] M. Adams *et al.*, “Tech. Report No. LBNL-6616E,” (2019).

[88] W. G. Cook, P. Figueras, M. Kunesch, U. Sperhake, and S. Tunyasuvunakool, Int. J. Mod. Phys. D **25**, 1641013 (2016), arXiv:1603.00362 [gr-qc].

[89] M. Alcubierre, S. Brandt, B. Bruegmann, D. Holz, E. Seidel, R. Takahashi, and J. Thornburg, Int. J. Mod. Phys. D **10**, 273 (2001), arXiv:gr-qc/9908012.

[90] F. Pretorius, Class. Quantum Grav. **22**, 425 (2005), gr-qc/0407110.

[91] J. Balakrishna, E. Seidel, and W.-M. Suen, Phys. Rev. D **58**, 104004 (1998), gr-qc/9712064.

[92] N. Sanchis-Gual, C. Herdeiro, and E. Radu, Class. Quant. Grav. **39**, 064001 (2022), arXiv:2110.03000 [gr-qc].

[93] M. Brito, C. Herdeiro, E. Radu, N. Sanchis-Gual, and M. Zilhão, Phys. Rev. D **107**, 084022 (2023), arXiv:2302.08900 [gr-qc].

[94] J. R. Oppenheimer and G. M. Volkoff, Phys. Rev. **55**, 374 (1939).

[95] R. C. Tolman, Phys. Rev. **55**, 364 (1939).

[96] G. B. Cook, S. L. Shapiro, and S. A. Teukolsky, The Astrophysical Journal **424**, 823 (1994).

[97] J. L. Friedman, J. R. Ipser, and R. D. Sorkin, The Astrophysical Journal **325**, 722 (1988).

[98] B. K. Harrison, K. S. Thorne, M. Wakano, and J. A. Wheeler, *Gravitation Theory and Gravitational Collapse* (Univers. Chicago Press, Chicago, 1965).

[99] N. Straumann, *General Relativity and Relativistic Astrophysics* (Springer, Berlin; New York, 1984).

[100] T. D. Lee and Y. Pang, Nucl. Phys. B **315**, 477 (1989).

[101] M. Gleiser, Phys. Rev. D **38**, 2376 (1988), [Erratum: Phys. Rev. D 39, 1257 (1989)].

[102] M. Gleiser and R. Watkins, Nucl. Phys. B **319**, 733 (1989).

[103] P. Jetzer, Nucl. Phys. B **316**, 411 (1989).

[104] P. Jetzer, Nucl. Phys. B Proc. Suppl. **14**, 265 (1990).

[105] P. Jetzer, Phys. Lett. B **222**, 447 (1989).

[106] E. Seidel and W.-M. Suen, Phys. Rev. D **42**, 384 (1990).

[107] M. Alcubierre, R. Becerril, S. F. Guzman, T. Matos, D. Nunez, and L. A. Urena-Lopez, Class. Quant. Grav. **20**, 2883 (2003), arXiv:gr-qc/0301105.

[108] N. M. Santos, C. L. Benone, and C. A. R. Herdeiro, JCAP **06**, 068 (2024), arXiv:2404.07257 [gr-qc].

[109] N. Sennett, T. Hinderer, J. Steinhoff, A. Buonanno, and S. Ossokine, Phys. Rev. D **96**, 024002 (2017), arXiv:1704.08651 [gr-qc].

[110] M. Okounkova, (2020), arXiv:2004.00671 [gr-qc].

[111] U. Sperhake, Phys. Rev. D **76**, 104015 (2007), gr-qc/0606079.

[112] T. Helfer, D. J. E. Marsh, K. Clough, M. Fairbairn, E. A. Lim, and R. Becerril, JCAP **1703**, 055 (2017), arXiv:1609.04724 [astro-ph].

[113] A. Toubiana, S. Babak, E. Barausse, and L. Lehner, Phys. Rev. D **103**, 064042 (2021), arXiv:2011.12122 [gr-qc].

[114] W. G. Cook and U. Sperhake, Class. Quant. Grav. **34**, 035010 (2017), arXiv:1609.01292 [gr-qc].